THERMALLY STRATIFIED BÖDEWADT FLOW OF HYBRID NANOFLUID

STUDENT NAME: ZARA MUSHTAQ SHAH
ENROLLMENT NO: 01-248202-011
SUPERVISOR: DR. JAFAR HASNAIN

A thesis submitted in fulfillment of the requirements for
the award of the degree of MS (Mathematics)

Department of Computer Science

BAHRIA UNIVERSITY ISLAMABAD

SEPTEMBER 2022

Approval of Examination

Scholar Name: Zara Mushtaq Shah

Registration Number: 71102

Enrollment: 01-248202-011

Program of Study: MS Mathematics

Thesis Title: Thermally stratified Bödewadt flow of hybrid nanofluid

It is to certify that the above scholar's thesis has been completed to my satisfaction and, to my belief, its standard is appropriate for submission for examination. I have also conducted plagiarism test of this thesis using HEC prescribed software and found similarity index 16 %. that is within the permissible limit set by the HEC for the MS/M. Phil degree thesis. I have also found the thesis in a format recognized by the BU for the MS/M.Phil thesis.

Supervisor Name: Dr. Jafar Hasnain

Supervisor Signature:

Date: September 30, 2022

Author's Declaration

I, Zara Mushtaq Shah hereby state that my MS/MPhil thesis titled "Thermally stratified Bödewadt flow of hybrid nanofluid" is my own work and has not been submitted previously by me for taking any degree from this university Bahria University or anywhere else in the country/world.

At any time if my statement is found to be incorrect even after my Graduate the university has the right to withdraw/cancel my MS/M.Phil degree.

Name of Scholar: ZARA MUSHTAQ SHAH

Date: September 30, 2022

Plagiarism Undertaking

I, solemnly declare that research work presented in the thesis titled "Thermally stratified Bödewadt flow of hybrid nanofluid" is solely my research work with no significant contribution from any other person. Small contribution/help wherever taken has been duly acknowledged and that complete thesis has been written by me.

I understand the zero tolerance policy of the HEC and Bahria University towards plagiarism. Therefore, I as an Author of the above titled thesis declare that no portion of my thesis has been plagiarized and any material used as reference is properly referred/cited.

I undertake that if I am found guilty of any formal plagiarism in the above titled thesis even after award of MS/M.Phil degree, the university reserves the right to withdraw / revoke my MS/M.Phil degree and that HEC and the University has the right to publish my name on the HEC/University website on which names of students are placed who submitted plagiarized thesis.

Name of Scholar: ZARA MUSHTAQ SHAH

Date: September 30, 2022

Dedication

I dedicate this thesis to my beloved parents and adoring siblings because whatever I am is just because of my parents and siblings prayers, love, unlimited support and their interest for the completion of my degree.

I also dedicate this to my respected supervisor Dr. Jafar Hasnain who has supported me and impressed me by his hard work, sincerity towards his profession, research skills and his method of mentoring research students.

Acknowledgments

Everlasting praise to ALLAH the most Gracious, the most merciful who bestowed me with His great blessings. He who says in the Quran,

“Indeed, I am near. I respond to the invocation of the supplicant when someone calls upon me.’’ (Surah AL-Baqarah; Ayat:186)

I am really blessed as He gave me the ability to think even upon a tiny thing He created. He gave me a source (His beloved Prophet (PBUH)) of light for my way to Him.

My acknowledgment is to my respected and sincere supervisor, Dr. Jafar Hasnain, who supported me with his significant opinions, research skills and inspirational thoughts towards education. I would acknowledge my teachers, in particular, Dr. Rizwan-ul-haq who encouraged me and helped me to see what I could be and Dr. Muhammad Ramzan who inspired me to become a good researcher.

I am grateful to my parents specially my mother whose guidance helped me throughout my life. I am also thankful to my both brothers Ishfaq Hussain Shah and Junaid Mushtaq Shah for their unlimited support to continue my degree in this university.

I would like to express my special thanks to PhD student Nomana Abid who was always remained helpful to me against every odd throughout my thesis and course work.

Abstract

Present thesis represents the in-depth research of thermally stratified Bödewadt flow of hybrid nanofluid (HNF) containing different shaped hybrid nanoparticles (NPs) past a stretching stationary disk surface including generalized slip condition along with the consequences of thermal stratification and heat source impacts. Behavior of hybrid thermo-physical features of CuO, Cu and Ag nanoparticles are analyzed past a stretching stationary disk frame. Two different shaped nanoparticles, namely CuO and Cu in spherical configuration and Ag in cylindrical shape are investigated in this analysis. Two different shaped hybrid models are taken into account in this research which are $CuO-Ag-water$ HNF and $Cu-Ag-water$ HNF. Uniqueness of this research work is supplemented by using the consequences of thermal stratification and heat source on thermally stratified Bödewadt flow of hybrid nanofluid. In this research work, the formulation is hybrid nanofluid (HNF) flow containing CuO, Cu and Ag NPs with BF water (H_2O) over a stretching stationary disk frame. Well suited transformations are employed to obtain dimensionless governing equations. Numerical solutions are achieved via shooting method with coexistence of Runge–Kutta (RK) method. Graphical illustrations are used to display the impacts of physical emergent variables on velocity, temperature, and concentration profiles. It is observed that the degradation of boundary layer (BL) thickness is significantly influenced by the uniform stretching of the disk. Prandtl number and stretching parameter are the physical parameters used in this research. Especially the typical Bödewadt BL is significantly changed by the stretching of the wall in the radial direction of the stationary disk. The thickness of the TBL is also observed to significantly drop even for moderate stretching strength as an outcome of the depletion in the momentum BL. This result is noteworthy from a technological standpoint since, in real-world applications, the radial stretching might help to cool down the system. However, this research analysis is useful for the progress point of view of a cooling system in an industrial sector, micro-manufacturing, for the treatment of cancer patients and in voltaic devices, hybrid-powered engines and solar energy applications in the real world.

TABLE OF CONTENTS

LIST OF TABLES

LIST OF FIGURES

LIST OF SYMBOLS

Symbols

r, θ, z	Spatial coordinates (m)
u, v, w	Velocity constitutes across r, θ and z (m/s)
F	Non-dimensional radial velocity $(-)$
G	Non-dimensional tangential velocity $(-)$
H	Non-dimensional axial velocity $(-)$
T	Temperature (K)
p	Pressure (N/m^2)
T_w	Convective surface temperature (K)
T_∞	Ambient fluid temperature (K)
T_0	Reference temperature (K)
Pr	Prandtl variable $(-)$
C_p	Specific heat capability (kJ/kgK)
S_t	Thermal stratification coefficient $(-)$
$(\rho C_p)_f$	Heat capability of fluid (J/K)
$(\rho C_p)_{nf}$	Heat capability of nanofluid (J/K)
$(\rho C_p)_{hnf}$	Heat capability of hybrid nanofluid (J/K)
C	Stretching parameter $(-)$
Q	Heat source variable (J)

Q^*	Non-dimensional heat source variable $(-)$
s	Stretching rate (m^2/s)
Nu	Nusselt number $(-)$
Nu_L	Local Nusselt variable $(-)$
Cf	Skin-friction parameter $(-)$
D, D_1	Thermal stratified dimensional constants (K)

Greek symbols

υ_{nf}	Nanofluid kinematic viscosity (m^2/s)
μ_{nf}	Viscosity of nanofluid (Ns/m^3)
α_{nf}	Thermal diffusion of nanofluid (m^2/s)
τ_W	Wall shear stress (Pa)
α^*	Navier's slip constant $(-)$
β^*	Corresponding of few basic shear transmission rate $(-)$
α	Non-dimensional velocity slip variable $(-)$
β	Non-dimensional critical shear transmission rate $(-)$
ϕ_i	Non-dimensional concentration $(-)$
η	Variable of dimensionless similarity $(-)$
k_{nf}	Thermal conductance of nanofluid (W/mK)
υ_{hnf}	Hybrid nanofluid kinematic viscosity (m^2/s)
θ	Dimensionless fluid temperature $(-)$
ρ	Density (kg/m^3)
μ	Dynamic viscosity (kg/ms)

k_{hnf}	Thermal conductance of hybrid nanofluid $\left(\mathrm{W}/mK\right)$
μ_{hnf}	Viscosity of hybrid nanofluid $\left(Ns/m^3\right)$
α_{hnf}	Heat diffusivity of hybrid nanofluid $\left(\mathrm{m}^2/s\right)$
Ω	Rotational parameter $\left(Rad/s\right)$

Subscripts

i	$i=1$ for CuO nanoparticles
	$i=2$ for Cu nanoparticles
	$i=3$ for Ag nanoparticles
	$i=CuO$ for copper oxide nanoparticles
	$i=Cu$ for copper nanoparticles
	$i=Ag$ for silver nanoparticles
t	For thermal
L	For local
r	For radial
ϑ	For tangential
W	$W=r$ for radial
	$W=\vartheta$ for tangential
w	For surface
∞	For ambient
0	For reference

Acronyms

NF	Nanofluid
HNF	Hybrid nanofluid
TBL	Thermal boundary layer
BL	Boundary layer
NP	Nanoparticle
BF	Base fluid

TC	Thermal conductivity
BC	Boundary condition
FF	Fluid flow
f	Fluid
nf	Nanofluid
hnf	Hybrid nanofluid

CHAPTER 1

INTRODUCTION

1.1 Overview

This chapter is intended to provide basic fluid ideas as well as definitions and equations in order to explain the flow analysis presented in the system.

The term "classical Bödewadt BL flow" refers to the three dimensional motion of flow caused by the rotation of a viscid fluid adequately enough away from a stationary disk. One of the more well-known fluid physics challenges where the motion is superimposed because the fluid is farther away from the stationary disk and rotating with a uniform angular speed. Less research has been done to grasp the physical insight of this case, despite the fact that it also has theoretical and practical significance, such as in understanding the dynamics of tornadoes and hurricanes and rotor stator systems in turbines. As a result, there has been extensive research on the three-dimensional rotating flow motion and energy generated by a stationary disk.

Nanoparticles (NPs) have advanced thermal implications in recent advanced nanotechnology developments, as they become increasingly significant in many engineering and thermal discharge technologies. NPs are nano-sized particles that can take the shape of carbon nanotubes, metals, or oxides and are used to improve thermal conductivity (TC) and heat transmission, because NPs have a far higher TC than the basic base fluid (BF). Recent nanofluid (NF) research demonstrates that the fluid characteristics change when NPs are added. NFs are the best substitute for conventional heat transfer base liquids in terms of TC. NFs are very efficient heat transfer fluids made by dispersing NPs with diameters smaller than 100 nm in conventional fluids such as water, it becomes nanofluid. NFs are solid-liquid composite substances that can transmit heat over large temperature differences. For heat transfer applications, these fluids gain metaphysical properties such as viscidity, consistency,

and specific heat, among others. NFs are used for the enhancement of TC using low concentration of NPs, they potent temperature parameter based on TC, and the nonlinear development in TC using NPs and augmentation in boiling crucial heat flux. Because of their improved TC and convective heat transfer factor, NFs have become more important. Over the past some decades, research on the topic of NF has been extensively growing fast. Because of their unique properties like thermal conductivity, nanofluids are mainly used in many fields like pharmacy, medical field and nuclear science technologies.

In addition, the team of researchers attempted to conduct study in the field of nanosciences using a hybrid nanofluid (HNF) approach, which is developed via dragging different NPs in composite or mixed configuration. The goal of employing HNFs is to improve the thermal transfer capabilities of nanomaterials by increasing their aspect ratio, dynamic work, and thermal network. HNFs are created by combining two or more unique NPs into the BF in order to increase the TC of the NF, which is higher than basic fluid or NFs with single particles. HNFs with polymeric, metallic or non-metallic NPs with a BF to increase heat transmission rates in various applications. Numerous researchers have demonstrated that the HNF has a higher heat transmission rate than BF, both experimentally and statistically. The thermo-physical qualities of HNFs have a significant impact on their behavior in engineering systems. In thermal sciences, dynamic viscosity and TC are the most important of these qualities.

The motion of the surrounding fluid remains at rest if one imagines a zero-thickness disk that admits a stress-free condition on its surface and rotates around its axis. It supports the obvious conclusion that the BC on the disk is crucial to the fluid motion. In situations when the fluid is made up of emulsions, suspensions, foams, or polymer solutions, slip condition also has some industrial applications. It is similarly difficult to apply the no-slip boundary criterion precisely in other cases where the wall surface is rough. The general Navier's condition, which states that the magnitude of relative slip is proportionate to the local shear stress through the slip length, thereby accurately captures the appropriate BC. The no-slip requirement may be well approximated by a partial slip condition if the typical

scale of roughness is small relative to the BL thickness. The rate of particle change and temperature distribution throughout the fluid are both significantly impacted by heat generation or absorption. Examples of this phenomenon include semiconductor wafers, electronic chips, and nuclear reactors.

Stratification is a system of layering, categorization, and classification. This method produces substantial results in heat and mass transfer analysis. Temperature variances, concentration discrepancies, and the presence of distinct fluids all contribute to stratification. When two different kinds of water vapours with different temperatures come together then thermal stratification occurs. In solar engineering, thermal stratification analysis is crucial since better stratification can lead to increased energy efficiency. Exploring the impact of thermal and solutal stratification in mixed convection flow through a surface at the same time is exciting. By limiting oxygen mixing in the bottom layer of the water through biological processes, thermal stratification generates anoxia. Network efficiency is enhanced by improved energy efficiency, which can be obtained by stratification. It has extensive applications in physical phenomena such as aerodynamic sheet extrusion, geophysics, heat exchangers, metallurgy processes, and engineering domains such as chemical engineering, petroleum engineering, ceramic engineering and biochemical engineering.

Thermo-physical capabilities vary with the change of shape, size, types, BF and concentration of silver NPs. In light of this, it is still unclear which NP is appropriate for a certain BF as well as which forms of nanoparticles are more likely to increase thermal conductivity and heat transfer rate. Many studies have highlighted the development of silver NPs with varied forms that have various benefits in many disciplines, such as medicine, since silver NPs have unique qualities like optical and catalytic capabilities. These capabilities of silver NPs rely on the size and shape of the created NPs, which are unique. When added to polymers, coatings, and textiles, copper and copper oxide nanoparticles function as an anti-biotic, anti-microbial, and anti-fungal agent. Dietary supplements made of high-strength metals and alloys that distribute their nutrients effectively.

In this research analysis the investigation is on thermally stratified Bödewadt flow of hybrid nanofluid containing different shaped hybrid nanoparticles above a stretching stationary disk surface including generalized slip condition with the consequences of thermal stratification and heat source impacts. Boundary layer thickness is significantly influenced by the uniform stretching of the disk. Two different shaped nanoparticles, namely CuO and Cu in spherical configuration and Ag in cylindrical shape are examined in this research study. Two different shaped hybrid models are taken into account in this research analysis which are $CuO-Ag-water$ HNF and $Cu-Ag-water$ HNF. It is noteworthy that this research analysis is useful for the progress point of view of a cooling system in an industrial sector, micro-manufacturing, for the treatment of cancer patients and in voltaic devices, hybrid-powered engines and solar energy applications.

1.2 Fluid mechanics

It is a subfield of mechanics that investigates the characteristics of fluid at motion and at static condition. In fluid mechanics, there are two groups as

1.2.1 Fluid statics

The investigation of fluid characteristics at rest is the focus of this area of fluid mechanics.

1.2.2 Fluid dynamics

The study of fluid flow characteristics in motion is the focus of this branch of fluid mechanics.

1.3 Fluid

Fluid is the continuous deformation of a substance caused by pressure**.** Liquids and gases are the two types of fluids that exist. Fluids have no distinct shape. Some examples of fluid are water, honey, oil, blood, paint, air, mercury and gasoline. Fluids are divided into two kinds as

1.3.1 Ideal fluid

A hypothetical fluid known as the "ideal fluid" does not exist in this physical world. It is also devoid of viscosity, i.e.,

$$\mu = 0. \tag{1.1}$$

1.3.2 Real fluid

Real fluids are viscous. Examples of real fluid are ketchup, honey, water, petrol and kerosene etc, having some viscosity, i.e.,

$$\mu \neq 0. \tag{1.2}$$

1.4 Nanofluid

A fluid called a NF comprises NPs, which are particles with a diameter of $1-100$ nm. These fluids are concentrations of dispersion of NPs in a BF. In NFs, metals, oxides, carbides, and carbon nanotubes are frequently used as NPs. Its goal is to enhance thermo-physical properties of BF.

1.5 Nanoparticles

Nano-sized particles are small particles with a diameter of $1-100$ nm. NPs can be made out of a variety of materials i.e., metals, oxides and carbon nanotubes. Carbon, copper, and titanium dioxide are some examples. NPs are used to improve TC and heat transmission because heat transmission of NPs is substantially higher than that of the BF.

1.6 Hybrid nanofluid

In order to increase the TC of the NF, which is higher than in base fluids or single particle NFs, two or more different NPs are mixed into the basic fluids to create HNFs. In order to increase the rate of heat transmission in various application processes, HNFs with

combined mixture of different metallic oxides, polymeric materials, or non-metallic oxides NPs in BF are used. In comparison to BF, the HNFs has a greater heat transmission rate.

1.7 Heat transfer

Heat transmission is the movement of molecules caused by the transformation of inertial forces.

1.8 Thermal radiation

Thermal radiation is a physical phenomenon in which energy is radiated in all dimensions by a surface layer in the form of electromagnetic radiation waves, travelling through the surface layer at the speed of light directly to its point of absorption of heat energy.

1.9 Thermal stratification

When two different kinds of flow with different temperatures come together then thermal stratification will occur.

1.10 Thermal conductivity

Thermal conductivity is a process of heat transmission due to the internal ability of any material.

1.11 Thermal diffusivity

To define time-dependent fluid conductive heat flow, the rate of TC to density and specific heat capacity are used. This dimensionless parameter indicates how quickly a substance reacts with change in temperature. Thermal diffusivity is denoted by (α).In numerical form, it is written as

$$\alpha = \frac{k}{\rho C_p}. \tag{1.3}$$

1.12 Axisymmetric flow

A flow in which the streamlines are symmetrically positioned around an axis in hydrodynamics and fluid mechanics. The streamlined pattern would appear in every longitudinal plane through all the axis or the fluid flow variables, such as velocity and pressure are not affected by the angular coordinate θ in an axisymmetric flow.

1.13 Symmetric flow

A flow moving around an axis of the object is referred as symmetric flow. The flow can be in a cylindrical pipe or an unbounded space, with a finite cavity. The assumption here is that the object is star-like in relation to a point on the axis of symmetry.

1.14 Rotational symmetry

The rotating symmetry of a shape describes how an object's shape remains the same when revolved on its own axis.

1.15 Basic laws

Equation of continuity

$$\boldsymbol{div}.\boldsymbol{V} = \nabla.\boldsymbol{V} = 0. \tag{1.4}$$

The momentum equation

$$\rho \frac{\boldsymbol{dV}}{\boldsymbol{dt}} = \boldsymbol{div}.\boldsymbol{\tau} + \rho \boldsymbol{b}. \tag{1.5}$$

The energy equation

$$\rho \boldsymbol{C}_p \frac{\boldsymbol{dT}}{\boldsymbol{dt}} = \boldsymbol{\tau}.\boldsymbol{L} - \boldsymbol{div}.\boldsymbol{q}. \tag{1.6}$$

In above equation $\boldsymbol{\tau}$ is Cauchy stress tensor and $\boldsymbol{L}$ is the velocity gradient. These are defined as

$$\boldsymbol{\tau} = -\boldsymbol{pI} + \boldsymbol{\mu A}_1, \tag{1.7}$$

If the vector happens to be the velocity vector, v, then the tensor is known as the velocity gradient, and expressed by

$$\boldsymbol{L} = \Delta \boldsymbol{V}, \tag{1.8}$$

where

$$\boldsymbol{A}_1 = \boldsymbol{L} + \boldsymbol{L}^T. \tag{1.9}$$

Where the matrix form of Cauchy stress tensor $\boldsymbol{\tau}$ is expressed as

$$\boldsymbol{\tau} = \begin{bmatrix} \boldsymbol{\tau_{xx}} & \boldsymbol{\tau_{xy}} & \boldsymbol{\tau_{xz}} \\ \boldsymbol{\tau_{yx}} & \boldsymbol{\tau_{yy}} & \boldsymbol{\tau_{yz}} \\ \boldsymbol{\tau_{zx}} & \boldsymbol{\tau_{zy}} & \boldsymbol{\tau_{zz}} \end{bmatrix}. \tag{1.10}$$

Where,

$$\begin{aligned}
&\tau_{xx} = 2\mu \frac{\partial v_r}{\partial r} - p\ , && \tau_{xy} = \mu\left(\frac{1}{r}\frac{\partial v_r}{\partial \theta} - \frac{v_\theta}{r} + \frac{\partial v_\theta}{\partial r}\right), && \tau_{xz} = 2\mu \frac{\partial v_z}{\partial r}, \\
&\tau_{yx} = \mu\left(\frac{\partial v_\theta}{\partial r} + \frac{1}{r}\frac{\partial v_r}{\partial \theta} - \frac{v_\theta}{r}\right), && \tau_{yy} = \mu\left(2\frac{1}{r}\frac{\partial v_\theta}{\partial \theta} + \frac{v_r}{r}\right) - p, && \tau_{yz} = \mu\left(\frac{\partial v_\theta}{\partial z} + \frac{1}{r}\frac{\partial v_z}{\partial \theta}\right), \\
&\tau_{zx} = 2\mu \frac{\partial v_r}{\partial z}, && \tau_{zy} = \mu\left(\frac{1}{r}\frac{\partial v_z}{\partial \theta} + \frac{\partial v_\theta}{\partial z}\right), && \tau_{zz} = 2\mu \frac{\partial v_z}{\partial z} - p.
\end{aligned} \tag{1.11}$$

CHAPTER 2

LITERATURE REVIEW

2.1 Overview

This chapter is intended to provide the study related to Bödewadt flow, NF, NPs, hybrid NF, thermal stratification, generalized slip condition, different shaped nanoparticles and heat source impacts.

The term "classical Bödewadt BL flow" refers to the three dimensional motion of flow caused by the rotation of a viscid fluid adequately enough away from a stationary disk. One of the more well-known fluid physics challenges where the motion is superimposed because the fluid is farther away from the stationary disk and rotating with a uniform angular speed. Less research has been done to grasp the physical observation of this case, despite the fact that it also has theoretical and practical significance, such as in interpreting the science behind the tornadoes and hurricanes and rotor stator systems in turbines. As a result, there has been extensive research on the three-dimensional rotating flow motion and energy generated by a stationary disk. Bödewadt [1] first time theoretically investigated the Bödewadt BL flow takes place because of a rotating flow past a stationary disk and it shows a complete analytical solution of the Navier–Stokes equations. Rafiq et al. [2] studied the impact of varying fluid capabilities on heat transmission in Bödewadt flow with wall suction. He observed that energy equation in Bödewadt flow can have physically suitable solution only when disk is spongy and the foremost objective is the numerical evaluation of Bödewadt flow and heat transmission past a spongy disk with varying fluid features. Muhammad et al. [3] examined the Bödewadt NF flow with the help of kerosene oil and water as BFs and he worked on the numerical investigation of entropy generation reduction in Bödewadt NF flow

with the help of single wall and multi wall carbon nanotubes with viscid dissipation impacts. Awais et al. [4] investigated the non-linear input-output fitting with multilayer perceptrons neural network for numerical investigation of heat transmission influences in Bödewadt flow past a porous disk. Mustafa et al. [5] explored the fluid applied stress first appears in a Bödewadt flow involving a Bingham fluid, whose viscosity coefficient permits an indirectly proportional temperature reliance. By assuming an isothermal surface temperature, the associated heat transmission mechanism is examined.

Nanofluids are solid-liquid composite substances that can transmit heat over large temperature differences. For heat transfer applications, these fluids gain metaphysical properties such as viscidity, consistency, and specific heat, among others. Over the past some decades, research on the topic of NF has been extensively growing fast. The term 'nanofluid' was first suggested by Choi [6] to increase the TC of the base liquid by suspending NPs in it. Joshi et al. [7] investigated the Bödewadt flow of a NF with magnetic effects in the existence of geothermal viscid effects. The influences of porousness on time dependent BL flow of NFs with magnetic effects and water as a BF past an equally heated stationary disk are also examined. Khan et al. [8] observed NF takes up area past a stretchable disk in a typical Bödewadt flow. The transport equations take into account both thermophoresis and Brownian motion. Physically acceptable conditions that account for zero NPs normal flux are used. Rafiq et al. [9] investigated the numerical evaluation of the Bödewadt slip flow of NF past a rough spongy area. The convective type conditions which are practically acceptable are utilized for this research work. Zhou et al. [10] examined the microbially NF flow containing gyrotactic micro-organisms past a stationary disk. The spinning of NF with water as a BF, which is located far from a solid disk, is what causes the flow to begin.

Nanoparticles (NPs) have developed thermal implications in recent advanced nanotechnology developments, as they become increasingly significant in many engineering and thermal discharge technologies. NPs are nano-sized particles that can take the shape of carbon nanotubes, metals, or oxides and are used to improve thermal conductivity (TC) and heat transmission because NPs have a far higher TC than the basic base fluid (BF). Recent

nanofluid (NF) research demonstrates that the fluid characteristics change when NPs are added. Hayat et al. [11] observed the numerical study of three dimensional Bödewadt flow of carbon nanomaterial. Single walled and multi walled CNTs are mixed in water and gasoline oil base-liquids with Darcy-Forchheimer spongy media past a stationary disk. In the radial direction the stationary disk is further linearly stretched. Heat transmission influences are evaluated in the existence of radiation and convection phenomena. Moreover, entropy and dissipation influences are also investigated. Hani et al. [12] observed an incompressible three dimensional MHD Bödewadt flow of Casson NF past a stationary stretching disk. Shah et al. [13] examined the three dimensional micro-polar NFs of single and multi-walled carbon nanotubes (CNTs) mixed in BFs like water and gasoline.

In addition, the team of researchers attempted to conduct study in the field of nano-sciences using a hybrid nanofluid (HNF) approach, which is developed via dragging different NPs in composite or mixed configuration. The goal of employing HNFs is to improve the thermal transfer capabilities of nanomaterials by increasing their aspect ratio, dynamic work, and thermal network. HNFs are created by combining two or more unique NPs into the BF in order to increase the TC of the NF, which is higher than basic fluid or NFs with single particles. HNFs with polymeric, metallic or non-metallic NPs with a BF to increase heat transmission rates in various applications. Numerous researchers have demonstrated that the HNF has a higher heat transmission rate than BF, both experimentally and statistically. The thermo-physical qualities of HNFs have a significant impact on their behavior in engineering systems. Hayat and Nadeem [14] researched on silver-copper oxide-water HNF for heat transmission enhancement. Qiu et al. [15] investigated about a review of recent advances in thermo-physical features at the nanoscale from solid state to colloids. Abbas et al. [16] explored the study of three dimensional stagnation point flow of HNF past an isotropic slip surface. Muneeshwaran et al. [17] studied the accountability of HNF in heat transmission phenomenon.

The motion of the surrounding fluid remains at rest if one imagines a zero-thickness disk that admits a stress-free condition on its surface and rotates around its axis. It supports

the obvious conclusion that the BC on the disk is crucial to the fluid motion. In situations when the fluid is made up of emulsions, suspensions, foams, or polymer solutions, slip condition also has some industrial applications. It is similarly difficult to apply the no-slip boundary criterion precisely in other cases where the wall surface is rough. The general Navier's condition, which states that the magnitude of relative slip is proportionate to the local shear stress through the slip length, thereby accurately captures the appropriate BC. The no-slip requirement may be well approximated by a partial slip condition if the typical scale of roughness is small relative to the BL thickness. Sahoo [18] observed the influences of slip on steady Bödewadt flow and heat transmission phenomena of an electrically conducting non-Newtonian fluid. Sahoo and Poncet [19] investigated the steady flow arising due to the rotation of a non-Newtonian fluid at a larger distance from a stationary disk is extended to the case where the disk surface admits partial slip. The constitutive equation of the non-Newtonian fluid is modeled by that for a Reiner–Rivlin fluid. Sahoo et al. [20] studied brief note on the computation of the Bödewadt flow with Navier slip boundary conditions. Abbas et al. [21] evaluated the impacts of thermal radiation on heat transmission in the TBL caused by a generalized form vortex flow of NF past an unbounded disk with generalized slip condition.

The rate of particle change and temperature distribution throughout the fluid are both significantly impacted by heat generation or absorption. Examples of this phenomenon include semiconductor wafers, electronic chips, and nuclear reactors. Hayat et al. [22] observed the melting heat transmission in stagnation point flow of NF towards a stretched surface with nonlinear thermal radiation and heat transmission phenomena. Hayat et al. [23] highlighted the key characteristics of entropy analysis for flow of Sisko fluid. Fluid motion in this problem is due to a stretched disk. The fluid features are explained here in the existence of nonlinear mixed convection Brownian motion and viscid dissipation. Abdal et al. [24] examined the heat and mass transmission of time dependent tangent hyperbolic NF flow across an extensible Riga wedge under the impacts of stagnation point, heat source, and activation energy. Irfan et al. [25] observed the theoretical analysis of new max flux theory and Arrehenius activation energy in Carreau NF with magnetic influence.

Awais et al. [26] studied the impacts of heat transmission in a Bodewadt flow above a penetrable disk numerically. The repercussions of internal heat generation and absorption, viscous dissipation, magnetic field, joule heating along with varying capabilities of the fluid are also examined as well.

Stratification is a system of layering, categorization, and classification. This method produces substantial results in heat and mass transfer analysis. Temperature variances, concentration discrepancies, and the presence of distinct fluids all contribute to stratification. When two different types of water vapours with different temperatures come together then thermal stratification occurs. In solar engineering, thermal stratification analysis is crucial since better stratification can lead to increased energy efficiency. Exploring the influence of thermal and solutal stratification in mixed convection flow through a surface at the same time is exciting. By limiting oxygen mixing in the bottom layer of the water through biological processes, thermal stratification generates anoxia. Network efficiency is enhanced by improved energy efficiency, which can be obtained by stratification. It has extensive applications in physical phenomena such as aerodynamic sheet extrusion, geophysics, heat exchangers, metallurgy processes, and engineering domains such as chemical engineering, petroleum engineering, ceramic engineering and biochemical engineering. Jafar et al. [27] examined heat transmission rate for non-Newtonian (Casson) fluid motion impacted by thermal stratification and thermal radiation to accomplish in the presence of vertically applied magnetic field normal to the disks.

Thermo-physical capabilities vary with the change of shape, size, types, BF and concentration of silver NPs. In light of this, it is still unclear which NP is appropriate for a certain BF as well as which forms of nanoparticles are more likely to increase thermal conductivity and heat transfer rate. Many studies have highlighted the development of silver NPs with varied forms that have various benefits in many disciplines, such as medicine, since silver NPs have unique qualities like optical and catalytic capabilities. These capabilities of silver NPs rely on the size and shape of the created NPs, that are unique. When added to polymers, coatings, and textiles, copper and copper oxide nanoparticles function as an anti-

biotic, anti-microbial, and anti-fungal agent. Dietary supplements made of high-strength metals and alloys that distribute their nutrients effectively. Raza et al. [28] observed the size- and shape dependent antibacterial studies of silver NPs synthesized by wet chemical processes. Sobamowo et al. [29] discussed the impacts of NP geometry, slip, and temperature jump conditions on thermo-magneto-solutal squeezing flow of NF between two parallel disks fixed in a spongy media. Dadsetani et al. [30] investigated the influence of copper oxide NPs in a radial configuration microchannel of a stationary disk from the mechanical and thermal points of view. Umavathi [31] discussed the influences of NPs with magnetic effects in the increase of heat transmission rate in a tri-biological system subjected to convective type heating (Robin) boundary conditions with porous lower disk and fixed upper disk.

Mustafa et al. [32] in this review work analyzed the Bödewadt flow and heat transmission in NFs and the problem formulation is totally based on the Tiwari and Das model. Mustafa [33] examined the conventional Bödewadt BL of an in-compressed nature viscid FF and heat transmission above a uniform disk with radial stretching. It is also discovered that when the Bödewadt boundary layers behaviour and stability properties are uniformly stretched in the radial direction, they are significantly impacted. Karman [34] examined the effects of laminar friction and turbulent friction and his famous transformations are used in this research analysis.

With this motivation of interpretative and inventive studies on NFs and HNFs, stratified Bödewadt flow of hybrid nanofluid is the objective of the current research work. It is noteworthy that this research analysis is useful for the advancement point of view of a cooling system in an industrial sector, micro-manufacturing, for the treatment of cancer patients and in voltaic devices, hybrid-powered engines and solar energy applications. Moreover, from aforementioned literature, there is no such study on Bödewadt flow with the effects of thermal stratification and concentration of different shaped NPs. So, the objective of the extension work is to study different shaped NPs in two types of HNFs in Bödewadt flow i.e., spherical shaped Cu and cylindrical shaped Ag in $Cu-Ag-water$ HNF and

spherical shaped CuO with cylindrical shaped Ag in $CuO-Ag-water$ HNF. In this research analysis the investigation is on thermally stratified Bödewadt flow of hybrid nanofluid containing different shaped hybrid nanoparticles above a stretching stationary disk surface including generalized slip condition with the consequences of thermal stratification and heat source impacts. Two different shaped nanoparticles, namely CuO and Cu in spherical configuration and Ag in cylindrical shape are examined in this research study. Two different shaped hybrid models are taken into account in this research analysis which are $CuO-Ag-water$ HNF and $Cu-Ag-water$ HNF.

CHAPTER 3

ON BÖDEWADT FLOW AND HEAT TRANSFER OF NANOFLUIDS OVER A STRETCHING STATIONARY DISK

3.1 Overview

This chapter represents the analysis on Bödewadt flow and heat transfer of NFs over a stretching stationary disk.

In this review work, the NF flow contains CuO in spherical formation, Cu with spherical configuration and Ag with also spherical structure NPs with BF H_2O past a stretching stationary disk. Behavior of thermo-physical characteristics of CuO, Cu and Ag NPs is analyzed above a stretching stationary disk model. Well suited transformations are employed to obtain dimensionless governing equations. Numerical solutions are obtained via shooting method with coexistence of Runge–Kutta (RK) method. Graphical illustrations are utilized to examine the consequences of physical emergent variables on velocity, temperature and concentration profiles. Pr, $C = \frac{s}{\Omega}$ and Cf are the emerging parameters used in this research study. This chapter is the review of research work done by Mustafa *et al.* [32].

3.2 Mathematical formulation

Consider the (r, ϑ, z) cylindrical coordinate system. Assume the NF with incompressible flow over a circular stretching stationary disk placed at $z = 0$. It is a 3 directional and 3 dimensional NF flow. The disk in the radial direction along with stretching rate is linearly stretched. The NF is a combination of 3 different CuO, Cu and Ag NPs with BF water (H_2O). The NF away from stretching stationary disk is spinning around a

disk with Ω like a rigid body. Far from the surface of the extending stationary disk, the fluid rotates like a solid body with a constant amount of Ω to produce the fluid motion around a disk. The components along the tangential direction represented by ϑ may also be disregarded because of the axial symmetry of the given model. Let the velocity components be regarded as $V=\left[u\left(r,z\right),v\left(r,z\right),w\left(r,z\right)\right]$ and temperature vector of system is represented by $T=T\left(r,z\right)$. We assumed the consistent temperature variable T_w at the surface of the stretching stationary disk and on the other side the consistent temperature variable T_∞ which is far away from the surface.

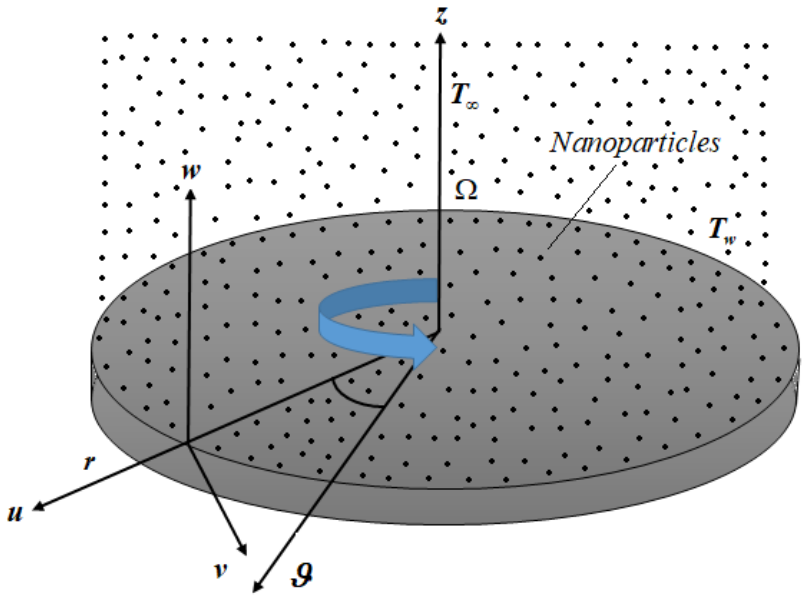

Figure 3.1: Physical depiction of the stretching stationary disk

Utilizing the Tiwari and Das given model [36], the mathematical system of momentum and heat equations in cylindrical coordinates for the present problem under the assumptions of boundary layer theory is given as

$$\frac{\partial u}{\partial r}+\frac{u}{r}+\frac{\partial w}{\partial z}=0, \tag{3.1}$$

$$\rho_{nf}\left(u\frac{\partial u}{\partial r}-\frac{v^2}{r}+w\frac{\partial u}{\partial z}\right)=-\frac{\partial p}{\partial r}+\mu_{nf}\left(\frac{\partial^2 u}{\partial z^2}\right), \tag{3.2}$$

$$\rho_{nf}\left(u\frac{\partial v}{\partial r}+\frac{uv}{r}+w\frac{\partial v}{\partial z}\right)=\mu_{nf}\left(\frac{\partial^2 v}{\partial z^2}\right), \tag{3.3}$$

$$u\frac{\partial T}{\partial r}+w\frac{\partial T}{\partial z}=\frac{k_{nf}}{\left(\rho C_p\right)_{nf}}\left(\frac{\partial^2 T}{\partial z^2}\right). \tag{3.4}$$

The associated BCs for above equations are given as

$$\left.\begin{aligned}u&=sr,\\ v&=0,\\ w&=0,\\ T&=T_w,\end{aligned}\right\} \quad at\ \ z=0, \qquad \left.\begin{aligned}u&=0,\\ v&=r\Omega,\\ T&\to T_\infty,\end{aligned}\right\} \quad as\ \ z\to\infty. \tag{3.5}$$

The thermophysical features of the NF model are represented below

$$\begin{aligned}&\mu_{nf}=\frac{\mu_f}{(1-\phi)^{2.5}},\ \alpha_{nf}=\frac{k_{nf}}{\left(\rho C_p\right)_{nf}},\ \rho_{nf}=(1-\phi)\rho_f+\phi\rho_s,\\ &\left(\rho C_p\right)_{nf}=(1-\phi)\left(\rho C_p\right)_f+\phi\left(\rho C_p\right)_s,\ \frac{k_{nf}}{k_f}=\frac{\left(k_s+2k_f\right)-2\phi\left(k_f-k_s\right)}{\left(k_s+2k_f\right)+\phi\left(k_f-k_s\right)}.\end{aligned} \tag{3.6}$$

Table 3.1: Thermophysical features of the BF (H_2O) and NPs CuO, Cu along with Ag

Thermo-physical features	H_2O	CuO	Cu	Ag
$\rho\left(kg/m^3\right)$	997.1	6320	8940	10500
$C_p\left(1/kgk\right)$	4179	531.5	385	233
$k\left(W/mk\right)$	0.613	76.5	400	429

At the frictionless domain, the radial pressure and the centrifugal force are balanced, as

$$\frac{1}{\rho_{nf}}\frac{\partial p}{\partial r}=r\Omega^{2}. \tag{3.7}$$

By using the following Von Karman transformations, similarity solutions for the flow equations can be constructed [34]

$$\begin{aligned}&\eta=\sqrt{\left(\frac{\Omega}{\nu_f}\right)}z,\quad u=r\Omega F(\eta),\quad v=r\Omega G(\eta),\quad w=\sqrt{\nu_f\Omega}H(\eta),\\&p=p_\infty+\rho\nu_f\Omega P(\eta),\qquad T=T_\infty+(T_w-T_\infty)\theta(\eta).\end{aligned} \tag{3.8}$$

Using the above Von Karman similarity transformations, the given mathematical system of NF model is transformed in the following system of equations

$$H'+2F=0, \tag{3.9}$$

$$\frac{1}{(1-\phi)^{2.5}\left(1-\phi+\phi\frac{\rho_s}{\rho_f}\right)}F''-HF'-F^2+G^2-1=0, \tag{3.10}$$

$$\frac{1}{(1-\phi)^{2.5}\left(1-\phi+\phi\frac{\rho_s}{\rho_f}\right)}G''-HG'-2FG=0, \tag{3.11}$$

$$\frac{\frac{k_{nf}}{k_f}}{\left(1-\phi+\phi\left(\frac{(\rho C_p)_s}{(\rho C_p)_f}\right)\right)}\frac{1}{Pr}\theta''-H\theta'=0, \tag{3.12}$$

the transformed BCs are

$$\left.\begin{aligned} H(0)&=0,\\ F(0)&=C,\\ G(0)&=0,\\ \theta(0)&=1, \end{aligned}\right\} \quad at \quad z=0, \qquad \left.\begin{aligned} F(\infty)&=0,\\ G(\infty)&=1,\\ \theta(\infty)&=0, \end{aligned}\right\} \quad as \quad z\to\infty. \tag{3.13}$$

The non-dimensional variables appearing in above equations are defined as

$$Pr=\frac{\left(\mu C_p\right)_f}{k_f} \quad and \quad C=\frac{s}{\Omega}. \tag{3.14}$$

The skin-friction co-efficient is represented as

$$Cf=\frac{\sqrt{\tau_r^2+\tau_\vartheta^2}}{\rho_f\left(r\Omega\right)^2}, \tag{3.15}$$

$$\tau_r=\mu_{nf}\frac{\partial u}{\partial z} \quad at \quad z=0, \qquad \tau_\vartheta=\mu_{nf}\frac{\partial v}{\partial z} \quad at \quad z=0. \tag{3.16}$$

Utilizing the Von Karman transformations [34] in above equations, we find the following infrastructure of equations as

$$\begin{aligned} &\tau_r=r\Omega\sqrt{\frac{\Omega}{\nu_f}}\frac{\mu_f}{\left(1-\phi\right)^{2.5}}F'(0), \qquad \tau_\vartheta=r\Omega\sqrt{\frac{\Omega}{\nu_f}}\frac{\mu_f}{\left(1-\phi\right)^{2.5}}G'(0),\\ &Cf=\sqrt{\frac{\nu_f}{r^2\Omega}}\frac{1}{\left(1-\phi\right)^{2.5}}\sqrt{F'(0)^2+G'(0)^2}. \end{aligned} \tag{3.17}$$

The below expression represents the local Nusselt number

$$Nu=\frac{rq_w}{k_f\left(T_w-T_\infty\right)}. \tag{3.18}$$

In above expression q_w represents the heat flow at the surface of stretched stationary disk which is given by

$$q_w = -k_{nf}\frac{\partial T}{\partial z} \quad at \quad z = 0. \tag{3.19}$$

Utilizing the Von Karman transformations [34] in above equations we find the following infrastructure of equations as

$$Nu = -\frac{k_{nf}}{k_f}\sqrt{\frac{r^2\Omega}{\nu_f}}\theta'(0). \tag{3.20}$$

3.3 Solution methodology

The shooting method combined with the RK procedure is employed to solve the nonlinear differential equations numerically which are in dimensionless form subject to the BCs mentioned in the Equations (3.9-3.13).

3.4 Numerical outcomes and discussion

In this research analysis the numerical solutions are obtained via shooting method with coexistence of Runge–Kutta (RK) method and coupled non-linear ODEs and transformed boundary conditions are solved with the help of this numerical approach.

Axial velocity components for numerous ϕ are plotted in Fig. 3.2. Furthermore, the outcomes for all three NPs CuO, Cu along with Ag are provided. Since a downward FF is expected due to stretching phenomenon, hence; the behavior of axial velocity $H(\eta)$ is downward i.e., the values of $H(\eta)$ are negative. It's intriguing to observe that as distance from disk rises, the axial component of velocity initially reaches a maximum point and then asymptotically reaches a consistent bounded value for $z \to \infty$. When we increase the amount of nanoparticles in the NF the axial velocity approaches to decline and it is high or low in the existence of nanoparticles of CuO and Ag.

The dependence of ϕ on the radial profile $F(\eta)$ is depicted in Fig. 3.3. The velocity component in the radial direction shows that the FF is radially in the outward direction close

to the disk and appears to be radially inward far away from the disk. ϕ and the velocity $F(\eta)$ in the radial position are inversely related.

For various values of ϕ the tangential velocity component $G(\eta)$ is presented in Fig. 3.4. The tangential profile $G(\eta)$ has a direct correlation with the volume percentage of NPs (ϕ) which includes concentration of all the nanoparticles CuO, Cu and Ag under consideration.

Fig. 3.5 shows the temperature profile which is represented by $\theta(\eta)$ for numerous values of ϕ. We see that a thicker TBL is correlated with enhancement in the ϕ. With given nanoparticle volume fraction (ϕ) of the silver-water $(Ag-water)$ NF exhibits the highest temperature profile $\theta(\eta)$ as compared to $Cu-water$ NF and $CuO-water$ NF.

Stretching effects over the Bödewadt BL for a constant volume percentage (ϕ) of NPs are depicted in Figs. 3.6-3.8. We see that the oscillatory properties of the circular component $F(\eta)$, divergent component $H(\eta)$, and central component $G(\eta)$ distributions are reduced as the stretching in the radial direction on the stationary disk increases. For verification glimpse into the Figs. 5-7.

When we increase the radial stretched rate which is represented by (s) on the plane of the stationary disk, the diameter of the BL starts decreasing. The radially outward FF is accelerated by an increase in the radially stretched rate which is validated in Fig. 3.7. As can be seen from the Fig. 3.6, this also increases the flow in the axial direction $H(\eta)$.

Furthermore, Fig. 3.9 shows the effect of stretching parameter C on temperature profile. It is observed that when radially stretched rate (s) of the stationary disk is significantly higher than the fluid rotation rate (Ω), the temperature parameter $\theta(\eta)$ penetration depth is reduced.

The consequence of the ϕ on the skin-friction coefficients $F'(0)$ and $G'(0)$ are illustrated in Figs. 3.10 and 3.11. A direct and nonlinear link is noted between ϕ and the magnitudes of skin- friction coefficients which are represented as $F'(0)$ and $G'(0)$.

Additionally, a significant behavior of skin-friction coefficients $|F'(0)|$ and $|G'(0)|$ is observed for the silver-water $(Ag-water)$ NF. With enhancement in the amount of ϕ the velocity in the upward position at a distance from the stationary disk minimizes when we take Cu and CuO NPs in BF water, which is represented in Fig. 3.12.

Fig. 3.13 represents the heat transmission rate from the given disk which increases when the NP fraction ϕ of copper and copper oxide NPs maximizes. Surprisingly, the heat transfer rate for the silver-water $(Ag-water)$ NF decreases as nanoparticle volume fraction (ϕ) maximizes from 0.1 to 0.2 such as $(0.1 \le \phi \le 0.2)$. The graphical illustrations of different variables on velocity curves and temperature curves are given below.

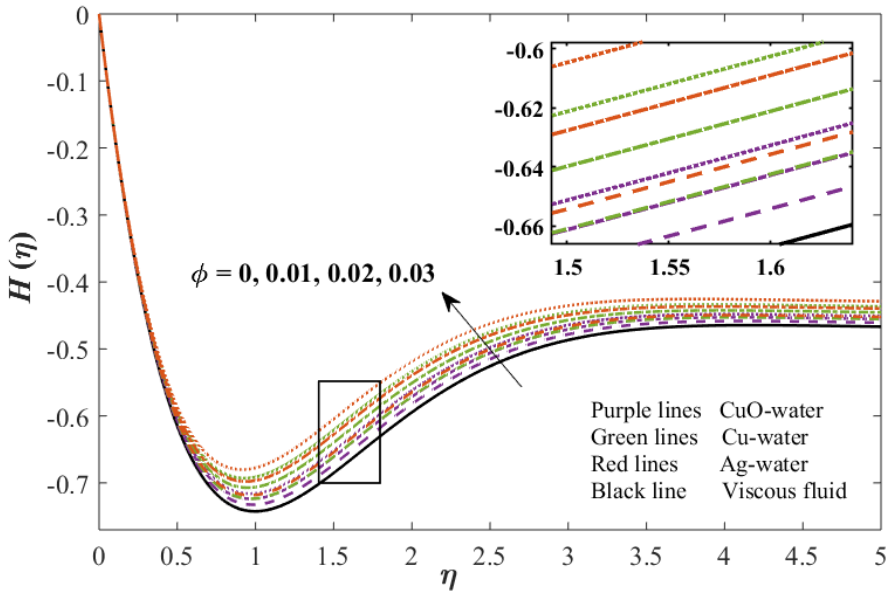

Figure 3.2: Behavior of $H(\eta)$ velocity against ϕ

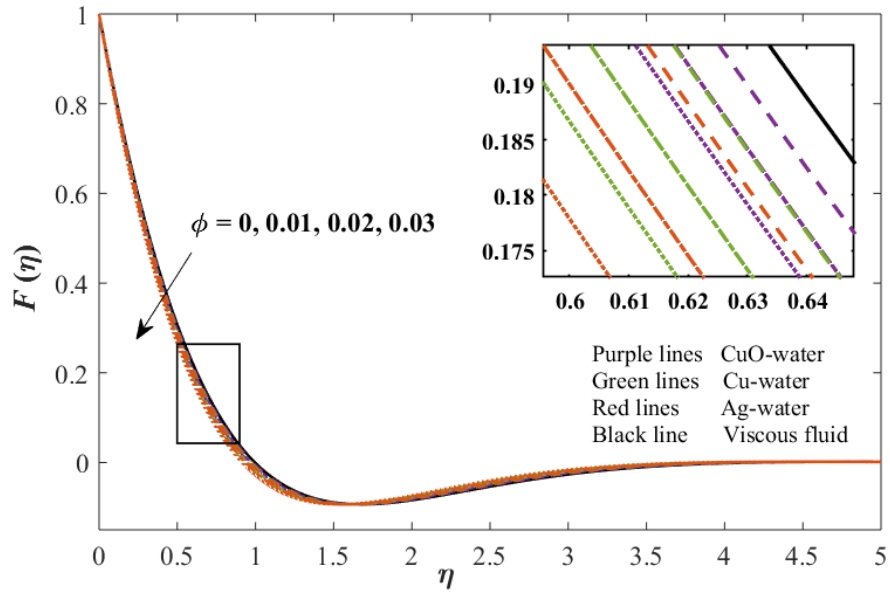

Figure 3.3: Behavior of $F(\eta)$ velocity against ϕ

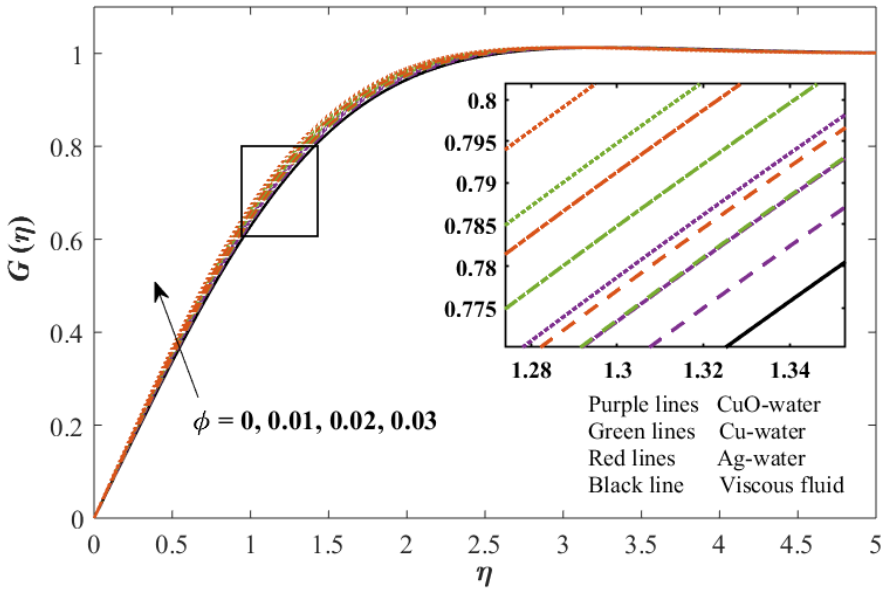

Figure 3.4: Behavior of $G(\eta)$ velocity against ϕ

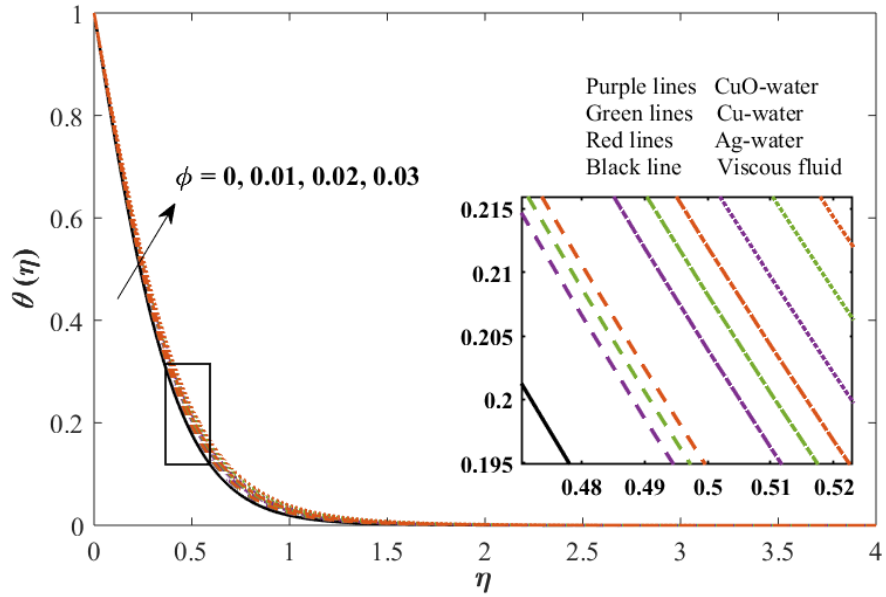

Figure 3.5: Behavior of $\theta(\eta)$ against ϕ

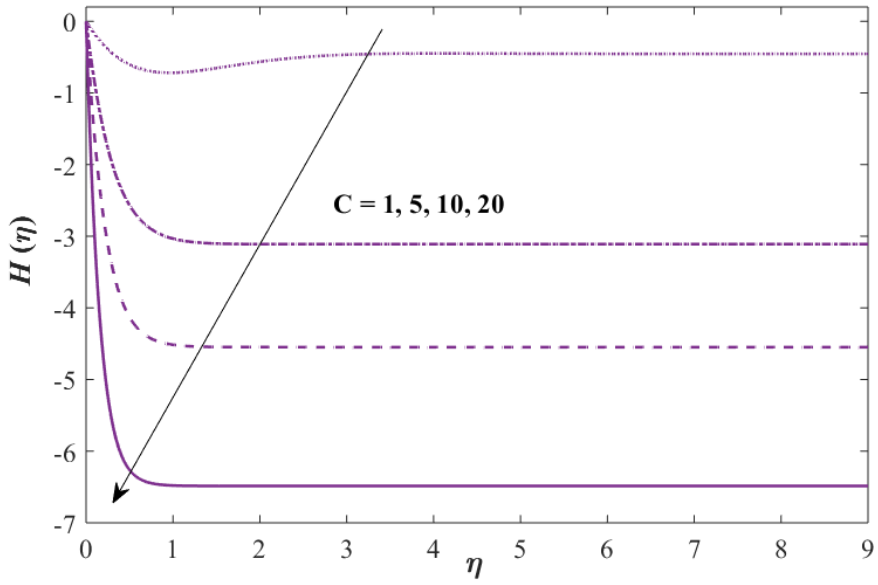

Figure 3.6: Behavior of $H(\eta)$ velocity against C

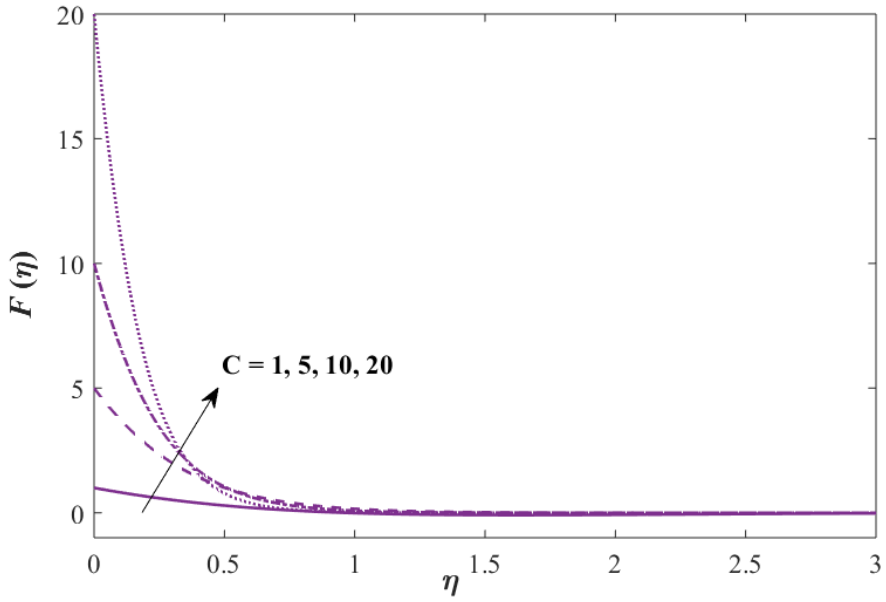

Figure 3.7: Behavior of $F(\eta)$ velocity against C

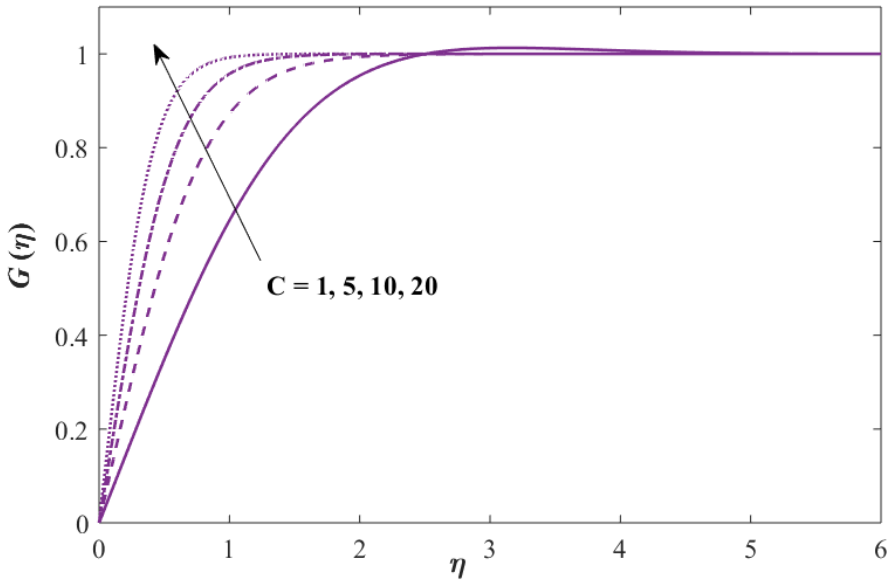

Figure 3.8: Behavior of $G(\eta)$ velocity against C

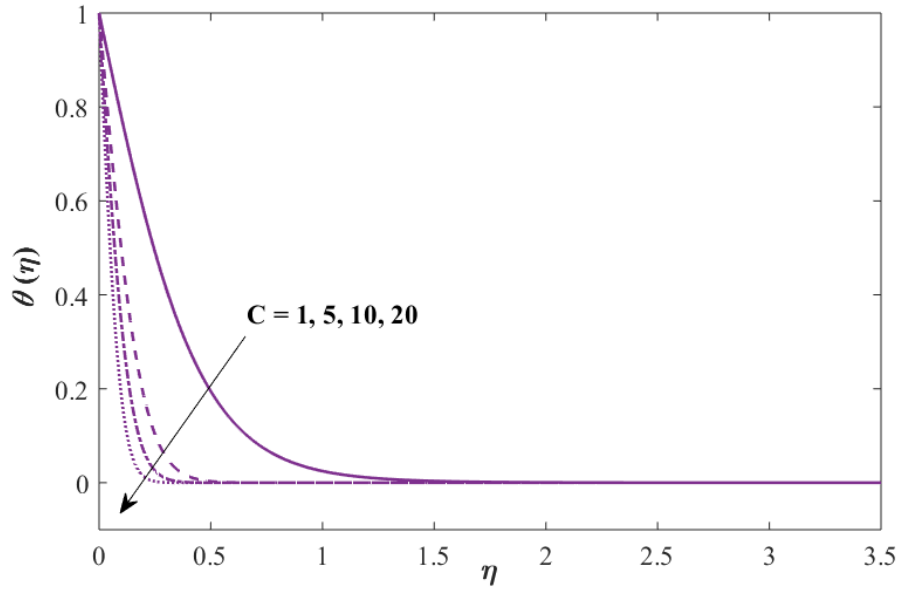

Figure 3.9: Behavior of $\theta(\eta)$ against C

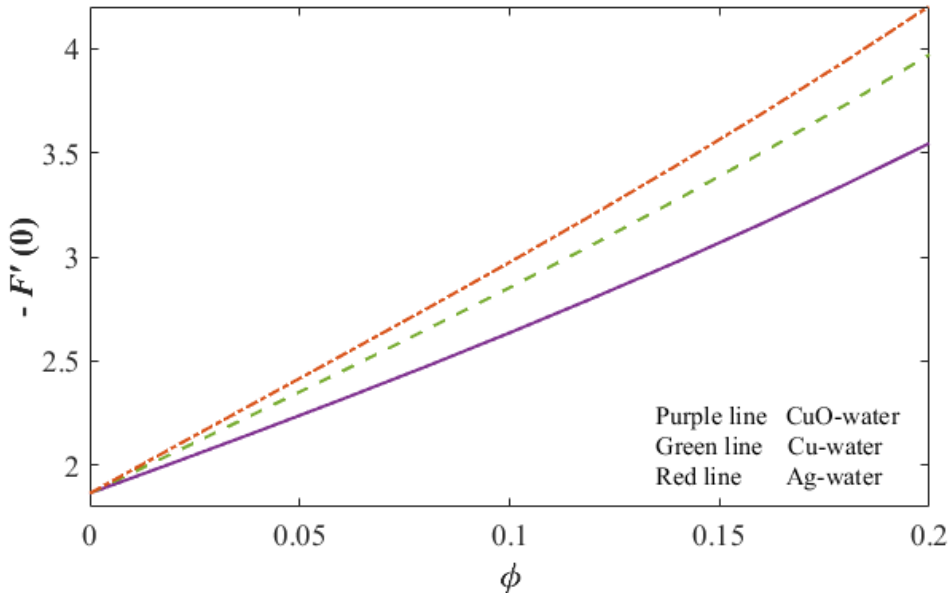

Figure 3.10: Behavior of $-F'(0)$ against ϕ

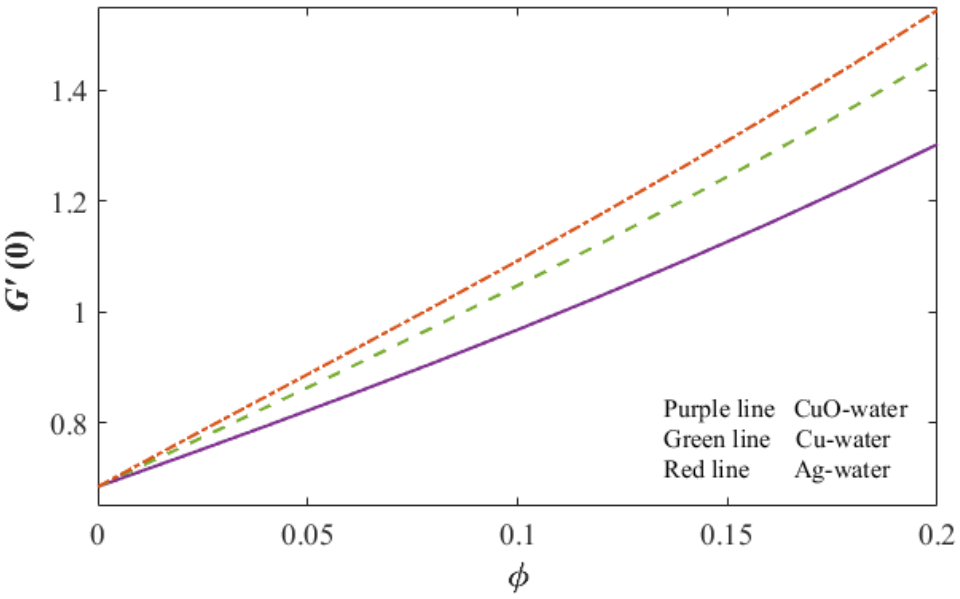

Figure 3.11: Behavior of $G'(0)$ against ϕ

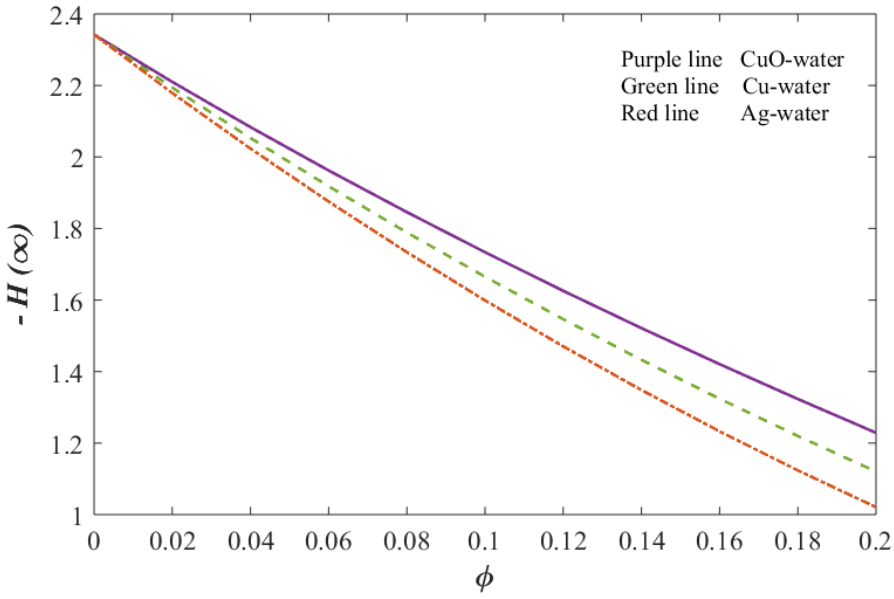

Figure 3.12: Behavior of $-H(\infty)$ against ϕ

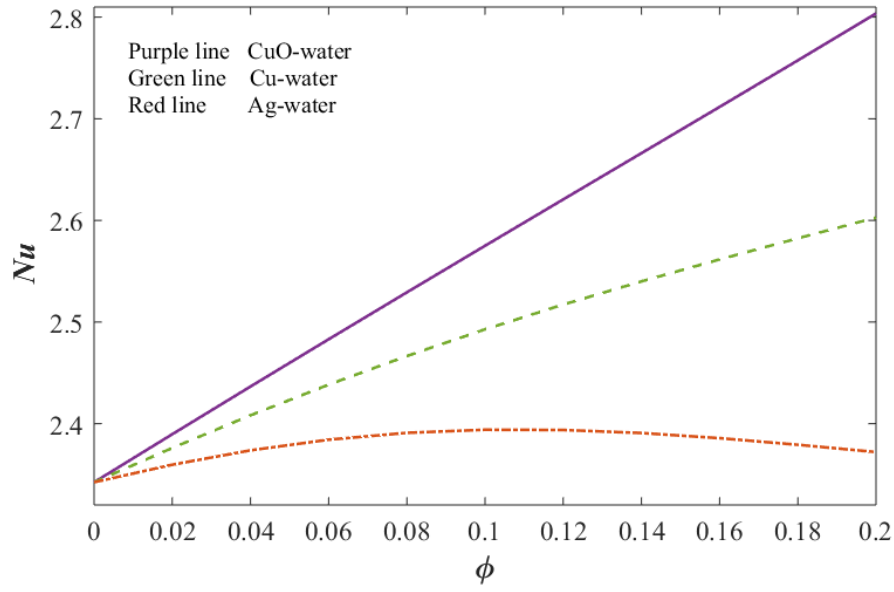

Figure 3.13: Behavior of Nu against ϕ

CHAPTER 4

THERMALLY STRATIFIED BÖDEWADT FLOW OF HYBRID NANOFLUID

4.1 Overview

In this chapter, the in-depth research of thermally stratified Bödewadt flow of hybrid nanofluid (HNF) containing different shaped hybrid nanoparticles (NPs) past a stretching stationary disk surface including generalized slip condition along with the consequences of thermal stratification and heat source impacts is discussed. Behavior of hybrid thermo-physical characteristics of CuO, Cu and Ag nanoparticles are analyzed over a stretching stationary disk frame. Two different shaped nanoparticles, namely CuO and Cu in spherical configuration and Ag in cylindrical shape are investigated in this analysis. Two different shaped hybrid models are taken into account in this research which are $CuO-Ag-water$ HNF and $Cu-Ag-water$ HNF. Uniqueness of this research work is supplemented by using the consequences of thermal stratification and heat source on thermally stratified Bödewadt flow of hybrid nanofluid. In this research work, the formulation is hybrid nanofluid (HNF) flow containing CuO, Cu and Ag NPs with BF water (H_2O) over a stretching stationary disk frame. Well suited transformations are employed to obtain dimensionless governing equations. Numerical solutions are obtained via

shooting method with coexistence of Runge–Kutta (RK) method. Graphical illustrations are used to display the impacts of physical emergent variables on velocity, temperature, and concentration profiles. It is observed that the degradation of boundary layer (BL) thickness is significantly influenced by the uniform stretching of the disk. Prandtl number, stretching parameter, heat source variable and thermal stratification parameter are the physical parameters used in this research. Especially the typical Bödewadt BL is significantly changed by the stretching of the wall in the radial direction of the stationary disk. The thickness of the TBL is also observed to significantly drop even for moderate stretching strength as an outcome of the depletion in the momentum BL. This result is noteworthy from a technological standpoint since, in real-world applications, the radial stretching might help to cool down the system. However, this research analysis is useful for the advancement point of view of a cooling system in an industrial sector, micro-manufacturing, for the treatment of cancer patients and in voltaic devices, hybrid-powered engines and solar energy applications in the real world.

4.2 Mathematical formulation

Assume (r,ϑ,z) cylindrical coordinate system with incompressible HNF flow in the presence of velocity slip above a circular stretching stationary disk placed at $z=0$. It is a 3 directional and 3 dimensional HNF flow. Moreover, the study consist of heat and momentum transport with heat source effects within both HNFs i.e., $CuO-Ag-water$ HNF and $Cu-Ag-water$ HNF. The disk is linearly stretching in the radial direction with stretching rate s. Two different shaped NPs, namely CuO and Cu in spherical configuration and Ag with cylindrical structure are considered in this research. Two different shaped hybrid nanofluids are taken into account in this analysis which are $CuO-Ag-water$ HNF and

$Cu-Ag-water$ HNF. The HNF away from stretching stationary disk is spinning around a disk with Ω like a rigid body. Far from the surface of the extending stationary disk, the fluid rotates like a solid body with a constant amount of Ω to produce the fluid motion around a disk. The components along the tangential direction represented by ϑ may also be disregarded because of the axial symmetry of the given model such that $\frac{\partial}{\partial \vartheta}=0$. Let the velocity components be regarded as $V=\left[u\left(r,z\right),v\left(r,z\right),w\left(r,z\right)\right]$ and temperature vector of system is represented by $T=T\left(r,z\right)$. We assumed the consistent temperature variable T_w at the surface of the stretching stationary disk and on the other side the consistent temperature variable T_∞ which is far away from the surface. The system of ODEs is then settled mathematically by utilizing numerical shooting technique with RK- method.

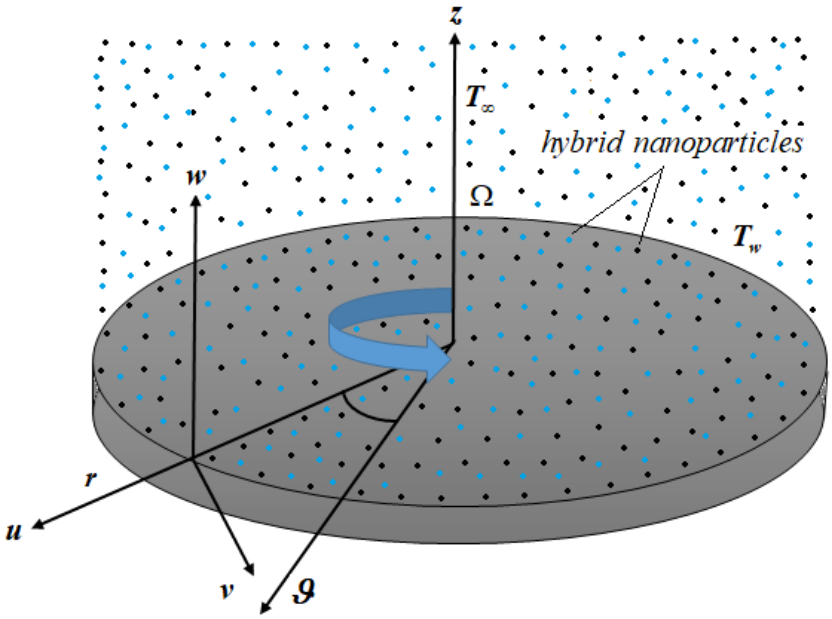

Figure 4.1: Physical depiction of HNFs over a stretching stationary disk

Utilizing the Tiwari and Das given model [36], the mathematical system of momentum and heat equations in cylindrical coordinates for the present problem under the assumptions of boundary layer theory are given as

$$\frac{\partial u}{\partial r}+\frac{u}{r}+\frac{\partial w}{\partial z}=0, \tag{4.1}$$

$$\rho_{hnf}\left(u\frac{\partial u}{\partial r}-\frac{v^2}{r}+w\frac{\partial u}{\partial z}\right)=-\frac{\partial p}{\partial r}+\mu_{hnf}\left(\frac{\partial^2 u}{\partial z^2}\right), \tag{4.2}$$

$$\rho_{hnf}\left(u\frac{\partial v}{\partial r}+\frac{uv}{r}+w\frac{\partial v}{\partial z}\right)=\mu_{hnf}\left(\frac{\partial^2 v}{\partial z^2}\right), \tag{4.3}$$

$$u\frac{\partial T}{\partial r}+w\frac{\partial T}{\partial z}=\frac{k_{hnf}}{\left(\rho C_p\right)_{hnf}}\left(\frac{\partial^2 T}{\partial z^2}\right)+\frac{Q\left(T-T_\infty\right)}{\left(\rho C_p\right)_{hnf}}, \tag{4.4}$$

with following given BCs

$$\left.\begin{aligned} &u=\alpha^*\left(1-\beta^*\frac{\partial u}{\partial z}\right)^{-\frac{1}{2}}\frac{\partial u}{\partial z}+sr,\\ &v=\alpha^*\left(1-\beta^*\frac{\partial v}{\partial z}\right)^{-\frac{1}{2}}\frac{\partial v}{\partial z},\\ &w=0, \quad T=T_w=T_0+D_1 r, \end{aligned}\right\} \quad at \quad z=0, \quad \left.\begin{aligned} &u=0,\\ &v=r\Omega,\\ &T=T_\infty=T_0+Dr, \end{aligned}\right\} \quad as \quad z\to\infty. \tag{4.5}$$

4.2.1 Thermo-physical properties of $CuO-Ag-water$ HNF

Mathematical models for the physical properties of $CuO-Ag-water$ HNF [35] are given below

$$\rho_{hnf}=\phi_1\rho_1+\phi_2\rho_2+\left(1-\phi_1-\phi_2\right)\rho_f, \tag{4.6}$$

$$\left(\rho C_p\right)_{hnf}=\phi_1\left(\rho C_p\right)_1+\phi_2\left(\rho C_p\right)_2+\left(1-\phi_1-\phi_2\right)\left(\rho C_p\right)_f, \tag{4.7}$$

$$\mu_{hnf}=\frac{\left(\mu_{nf_1}\phi_1+\mu_{nf_2}\phi_2\right)}{\left(\phi_1+\phi_2\right)}, \tag{4.8}$$

where,

$$\mu_{nf_1} = \left(\frac{\mu_f}{(1-\phi_1)^{2.5}} \right), \tag{4.9}$$

$$\mu_{nf_2} = \mu_f \left(1 + 13.5\phi_2 + 904.4\phi_2^2\right), \tag{4.10}$$

$$k_{hnf} = \left(\frac{k_{nf_1}\phi_1 + k_{nf_2}\phi_2}{\phi_1 + \phi_2} \right), \tag{4.11}$$

where,

$$\frac{k_{nf_1}}{k_f} = \frac{k_1 + (n-1)k_f - (n-1)(k_f - k_1)\phi_1}{k_1 + (n-1)k_f + (k_f - k_1)\phi_1}, \tag{4.12}$$

$$\frac{k_{nf_2}}{k_f} = \frac{k_2 + (n-1)k_f - (n-1)(k_f - k_2)\phi_2}{k_2 + (n-1)k_f + (k_f - k_2)\phi_2}. \tag{4.13}$$

4.2.2 Thermo-physical properties of $Cu - Ag - water$ HNF

Mathematical models for the physical properties of $Cu - Ag - water$ HNF [35] are given below

$$\rho_{hnf} = \phi_1\rho_1 + \phi_2\rho_2 + (1 - \phi_1 - \phi_2)\rho_f, \tag{4.14}$$

$$(\rho C_p)_{hnf} = \phi_1 (\rho C_p)_1 + \phi_2 (\rho C_p)_2 + (1 - \phi_1 - \phi_2)(\rho C_p)_f, \tag{4.15}$$

$$\mu_{hnf} = \frac{(\mu_{nf_1}\phi_1 + \mu_{nf_2}\phi_2)}{(\phi_1 + \phi_2)}, \tag{4.16}$$

where,

$$\mu_{nf_1} = \left(\frac{\mu_f}{(1-\phi_1)^{2.5}} \right), \tag{4.17}$$

$$\mu_{nf_2} = \mu_f \left(1+13.5\phi_2 + 904.4\phi_2^2\right), \tag{4.18}$$

$$k_{hnf} = \left(\frac{k_{nf_1}\phi_1 + k_{nf_2}\phi_2}{\phi_1 + \phi_2} \right), \tag{4.19}$$

where,

$$\frac{k_{nf_1}}{k_f} = \frac{k_1 + (n-1)k_f - (n-1)(k_f - k_1)\phi_1}{k_1 + (n-1)k_f + (k_f - k_1)\phi_1}, \tag{4.20}$$

$$\frac{k_{nf_2}}{k_f} = \frac{k_2 + (n-1)k_f - (n-1)(k_f - k_2)\phi_2}{k_2 + (n-1)k_f + (k_f - k_2)\phi_2}, \quad n = \frac{3}{\psi}. \tag{4.21}$$

For spherical shaped copper (Cu) and copper-oxide (CuO) nanoparticles $\psi = 1$,

for cylindrical shaped silver (Ag) nanoparticles $\psi = 0.62$.

Table 4.1: Thermophysical features of the BF (H_2O) and NPs i.e., CuO, Cu and Ag [32, 35]

Thermo-physical features	H_2O	$CuO(\phi_1)$	$Cu(\phi_1)$	$Ag(\phi_2)$
$\rho(kg/m^3)$	997.1	6320	8940	10500
$C_p(1/kgk)$	4179	531.5	385	233
$k(W/mk)$	0.613	76.5	400	429

At the frictionless domain, the radial pressure and the centrifugal force are balanced, as

$$\frac{1}{\rho_{hnf}} \frac{\partial p}{\partial r} = r\Omega^2. \tag{4.22}$$

By using the following Von Karman transformations [34], similarity solutions for the flow equations can be constructed

$$\eta = \sqrt{\left(\frac{\Omega}{\nu_f}\right)} z,\ u = r\Omega F(\eta),\ v = r\Omega G(\eta),\ w = \sqrt{\nu_f \Omega} H(\eta),$$
$$p = p_\infty + \rho \nu_f \Omega P(\eta),\ T = T_\infty + (T_w - T_0)\theta(\eta). \tag{4.23}$$

Using the above Von Karman similarity transformations, the given mathematical system of HNFs models is transformed in the following system of equations

$$H' + 2F = 0, \tag{4.24}$$

$$\frac{\mu_{hnf}}{\mu_f}\frac{\rho_f}{\rho_{hnf}} F'' - HF' - F^2 + G^2 - 1 = 0, \tag{4.25}$$

$$\frac{\mu_{hnf}}{\mu_f}\frac{\rho_f}{\rho_{hnf}} G'' - HG' - 2FG = 0, \tag{4.26}$$

$$\frac{k_{hnf}}{k_f}\frac{1}{Pr}\theta'' - \frac{(\rho C_p)_{hnf}}{(\rho C_p)_f}(S_t F + H\theta') + Q^*(S_t + \theta) = 0, \tag{4.27}$$

the converted BCs of the given HNFs models are

$$\left.\begin{aligned} &H(0) = 0,\\ &F(0) = \alpha\left(1 - \beta F'(0)\right)^{-\frac{1}{2}} F'(0) + C,\\ &G(0) = \alpha\left(1 - \beta G'(0)\right)^{-\frac{1}{2}} G'(0),\\ &\theta(0) = 1 - S_t, \end{aligned}\right\} \quad at \quad z = 0, \qquad \left.\begin{aligned} &F(\infty) = 0,\\ &G(\infty) = 1,\\ &\theta(\infty) = 0, \end{aligned}\right\} \quad as \quad z \to \infty. \tag{4.28}$$

The non-dimensional variables appearing in above equations are defined as

$$Q^* = \frac{Q}{(\rho C_p)_f \Omega}, \qquad C = \frac{s}{\Omega}, \qquad Pr = \frac{(\mu C_p)_f}{k_f}, \text{ and } \qquad S_t = \frac{D}{D_1}. \tag{4.29}$$

The skin-friction co-efficient is represented as follows

$$Cf = \frac{\sqrt{\tau_r^2 + \tau_\vartheta^2}}{\rho_f \left(r\Omega\right)^2}, \tag{4.30}$$

$$\tau_r = \mu_{hnf} \frac{\partial u}{\partial z} \quad at \quad z = 0, \qquad \tau_\vartheta = \mu_{hnf} \frac{\partial v}{\partial z} \quad at \quad z = 0. \tag{4.31}$$

Utilizing the Von Karman transformations [34] in structure of equations, we find the following infrastructure of equations as

$$\begin{aligned} &\tau_r = r\Omega \sqrt{\frac{\Omega}{\nu_f}} \frac{\mu_f}{\left(1-\phi\right)^{2.5}} F'(0), \qquad \tau_\vartheta = r\Omega \sqrt{\frac{\Omega}{\nu_f}} \frac{\mu_f}{\left(1-\phi\right)^{2.5}} G'(0), \\ &Cf = \sqrt{\frac{\nu_f}{r^2\Omega}} \frac{1}{\left(1-\phi\right)^{2.5}} \sqrt{F'(0)^2 + G'(0)^2}. \end{aligned} \tag{4.32}$$

The below expression represents the local Nusselt number

$$Nu = \frac{r q_w}{k_f \left(T_w - T_\infty\right)}, \tag{4.33}$$

In above expression q_w represents the heat flow at the surface of the stretched stationary disk which is given by

$$q_w = -k_{hnf} \frac{\partial T}{\partial z} \quad at \quad z = 0. \tag{4.34}$$

Utilizing the Von Karman transformations [34] in above equation we find the following non dimensional equation for heat rate.

$$Nu = -\frac{k_{hnf}}{k_f} \sqrt{\frac{r^2\Omega}{\nu_f}} \theta'(0). \tag{4.35}$$

4.3 Solution methodology

The shooting method combined with the RK procedure is employed to solve the nonlinear differential equations numerically which are in dimensionless form subject to the BCs mentioned in the Equations (4.24-4.28).

4.4 Numerical outcomes and discussion

In this research analysis the numerical solutions are obtained via shooting method with coexistence of Runge–Kutta (RK) method and coupled non-linear ODEs and transformed boundary conditions are solved with the help of this numerical approach.

Axial velocity component for various CuO and Cu nanoparticle volume fraction (ϕ_1) values are shown in Fig. 4.2. Furthermore, the outcomes for all the two HNF models $(CuO-Ag-water)$ HNF and $(Cu-Ag-water)$ HNF are provided here. Since a downward FF is expected due to stretching phenomenon, hence; the behavior of axial velocity $H(\eta)$ is downward i.e., the values of $H(\eta)$ are negative. It's intriguing to observe that as distance from disk rises, the axial component of velocity initially reaches a maximum point and then asymptotically reaches a consistent bounded value for $z\to\infty$. When we increase the amount of NPs CuO and Cu in the HNF, the axial curve $H(\eta)$ declines and it is more significant in the case of $(CuO-Ag-water)$ HNF model and low in the case of $(Cu-Ag-water)$ HNF over a stretching disk. The long distance $(\eta_{max}=10)$ that was determined to be sufficient to meet the unbounded boundary restrictions for both velocity curves and temperature fields was used to complete all the numerical values computations.

The dependence of spherical shaped CuO and Cu NP volume fraction (ϕ_1) on the radial velocity $F(\eta)$ is depicted in Fig. 4.3. The velocity profile in the radial position shows that the flow is radially outward close to the disk and appears to be radially inward far away from the stationary stretched disk. The CuO and Cu NP volume fraction (ϕ_1) and the

velocity $F(\eta)$ in the radial position are directly related. When we maximize the amount of CuO and Cu NP volume fraction (ϕ_1) the radial curve $F(\eta)$ also maximizes. Furthermore, it is high in the case of $Cu-Ag-water$ HNF model and low in the consequence of $CuO-Ag-water$ HNF model.

For numerous values of spherical shaped CuO and Cu with spherical configuration ϕ_1, the tangential velocity curves $G(\eta)$ are presented in Fig. 4.4. The tangential velocity curve $G(\eta)$ has an inverse correlation with the CuO and Cu NP volume fraction ϕ_1 which includes $CuO-Ag-water$ HNF and $Cu-Ag-water$ HNF model under consideration. When we maximize the amount of CuO and Cu NP volume fraction (ϕ_1) the tangential curve $G(\eta)$ decreases. Moreover, it is high in the consequence of $CuO-Ag-water$ HNF model and low in the scenario of $Cu-Ag-water$ HNF model.

Fig. 4.5 shows the temperature curves which are represented by $\theta(\eta)$ for numerous values of spherical shaped CuO and Cu NP volume fraction (ϕ_1). We see that a thicker TBL is correlated with enhancement in the amount of spherical shaped CuO and Cu NP volume fraction (ϕ_1). The increase in the concentration of nanoparticle (ϕ_1) of the $Cu-Ag-water$ HNF exhibits the highest temperature profile $\theta(\eta)$ as compared to the volume fraction of CuO in $CuO-Ag-water$ HNF.

Axial velocity curves for numerous values of silver NP volume fraction (ϕ_2) are shown in Fig. 4.6. The consequences for all the two HNF models $CuO-Ag-water$ HNF and $Cu-Ag-water$ HNF are presented here. When we increase the amount of nanoparticles Ag in the HNF the axial velocity $H(\eta)$ falls and it is high in the case of $CuO-Ag-water$ HNF and low in the case of $Cu-Ag-water$ HNF.

The dependence of the silver NP volume fraction (ϕ_2) on the radial velocity $F(\eta)$ is depicted in Fig. 4.7. The velocity curve in the radial direction shows that the FF is radially

outward close to the disk and appears to be radially inward at a given distance from the fixed disk. The concentration of cylindrical shaped silver NPs (ϕ_2) on the radial velocity $F(\eta)$ in the radial direction are directly related with each other. When we increase the amount of Ag NP volume fraction (ϕ_2) the radial curve $F(\eta)$ also increases. Moreover, it is maximum in the case $Cu-Ag-water$ HNF and minimum in the scenario of $CuO-Ag-water$ HNF.

For numerous values of Ag ϕ_2 the tangential velocity curves $G(\eta)$ are presented in Fig. 4.8. The tangential velocity curve $G(\eta)$ has an inverse correlation with the Ag nanoparticle fraction(ϕ_2) which includes both the $CuO-Ag-water$ HNF and $Cu-Ag-water$ HNF under examination. When we maximize the quantity of Ag nanoparticle concentration (ϕ_2) the tangential velocity $G(\eta)$ declines, it is high in the case of $CuO-Ag-water$ HNF as compared to $Cu-Ag-water$ HNF in Bödewadt flow.

Fig. 4.9 represents the clear image of the temperature profiles which are represented by $\theta(\eta)$ for numerous values of Ag ϕ_2. We see that a thicker TBL is in relation with enhancement in the amount of cylindrical shaped silver NPs (ϕ_2) nanoparticle volume fraction of copper particles in copper-silver-water $(Cu-Ag-water)$ HNF exhibits the highest temperature profile $\theta(\eta)$ as compared to the copper oxide-silver-water $(CuO-Ag-water)$ HNF flow past a stretched immovable disk.

The change in axial velocity curve $H(\eta)$ with the change in slip variable (α) is shown in Fig. 4.10. When we maximize the values of α the central velocity increases. It is high in the scenario of copper oxide-silver-water $(CuO-Ag-water)$ HNF and low in the consequence of copper-silver-water $(Cu-Ag-water)$ HNF.

The variation in radial velocity curve $F(\eta)$ with change in slip variable which is represented by α is plotted in Fig. 4.11. When we maximize the amount of slip parameter α, additional fluid can slip past the stationary disk and when we maximize the values of α

the radial velocity $F(\eta)$ decreases. Moreover, it is maximum in the case of $Cu-Ag-water$ HNF and minimum in the scenario of $CuO-Ag-water$ HNF past a stretching fixed disk.

The behavior of tangential velocity curve $G(\eta)$ with change in slip parameter α is shown in Fig. 4.12. When we maximize the values of α, the tangential velocity maximizes. Moreover, it is high in the scenario of $CuO-Ag-water$ HNF and low in the consequence of $Cu-Ag-water$ HNF.

Fig. 4.13 represents the variation in the axial velocity profile $H(\eta)$ with changing behavior in slip parameter β. When we increase the values of β, the axial velocity $H(\eta)$ declines. It is more significant in the consequence of $CuO-Ag-water$ HNF and low in the scenario of $Cu-Ag-water$ HNF.

Fig. 4.14 validates the behavior of radial velocity profile $F(\eta)$ with the different values of slip coefficient β. When we increase the amount of slip parameter β, additional fluid can slip past the stationary disk and the radial component $F(\eta)$ maximizes. It is maximum in the scenario of $Cu-Ag-water$ HNF while minimum in the case of $CuO-Ag-water$ HNF.

The effects of tangential velocity component $G(\eta)$ with different values of slip variable α is validated in Fig. 4.15. When we maximize the values of β, the tangential curve increases. It is more significant in the case of $CuO-Ag-water$ HNF and minimum when we take $Cu-Ag-water$ HNF flow past a stationary stretched disk.

The influence of thermal stratification parameter which is represented by S_t on temperature component (θ) is validated in Fig. 4.16. The temperature profile (θ) is a declining curve for maximizing values of S_t. A fall in temperature curve can be seen because the stratification process results in a variation among the wall and atmospheric fluid

temperature which is defined by T_∞. When we maximize the values of S_t, the thermal curves for the $CuO-Ag-water$ HNF decreases more as compared to $Cu-Ag-water$ HNF flow.

Fig. 4.18 represents the impact of heat source variable which is denoted by Q on temperature component (θ). The temperature component (θ) is a decreasing function of heat source phenomenon. When we increase the values of Q, the temperature profiles for $CuO-Ag-water$ HNF shows the significant decreasing behavior as compared to $Cu-Ag-water$ HNF. When the value of Q is greater than 0 it represents the circumstance in which there is a heat source, and case when the value of Q is less than 0 it represents the situation in which there is a heat sink. The graphical illustrations of various parameters on velocity curves and temperature curves are given below.

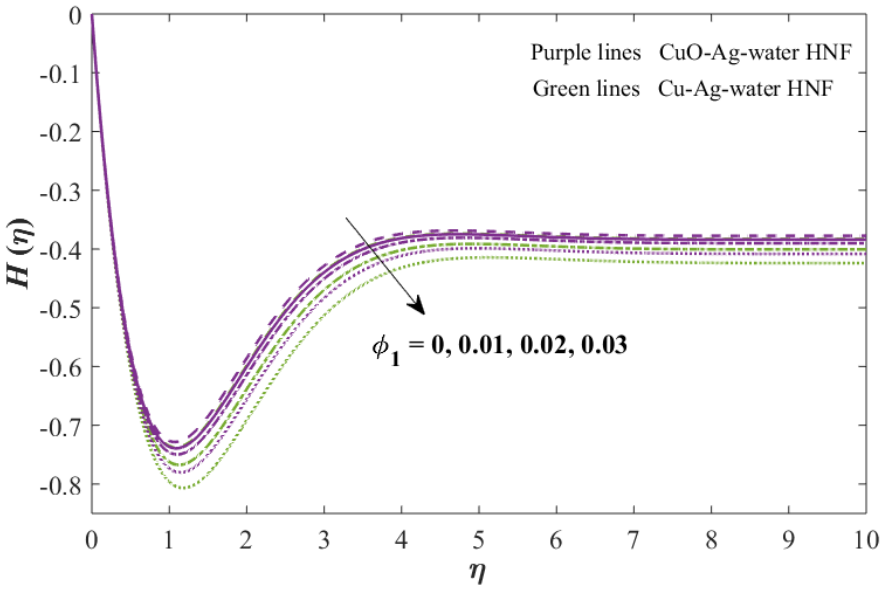

Figure 4.2: Behavior of $H(\eta)$ against ϕ_1

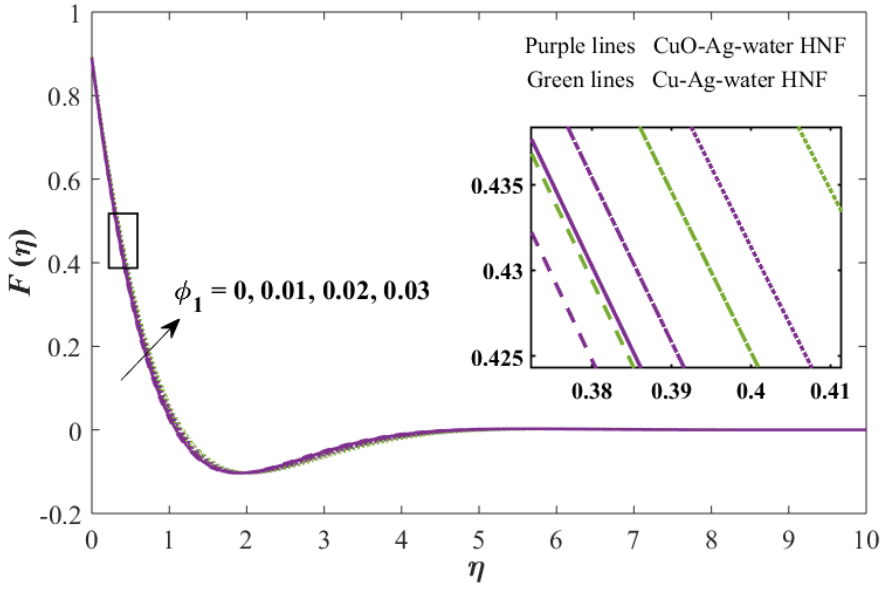

Figure 4.3: Behavior of $F(\eta)$ against ϕ_1

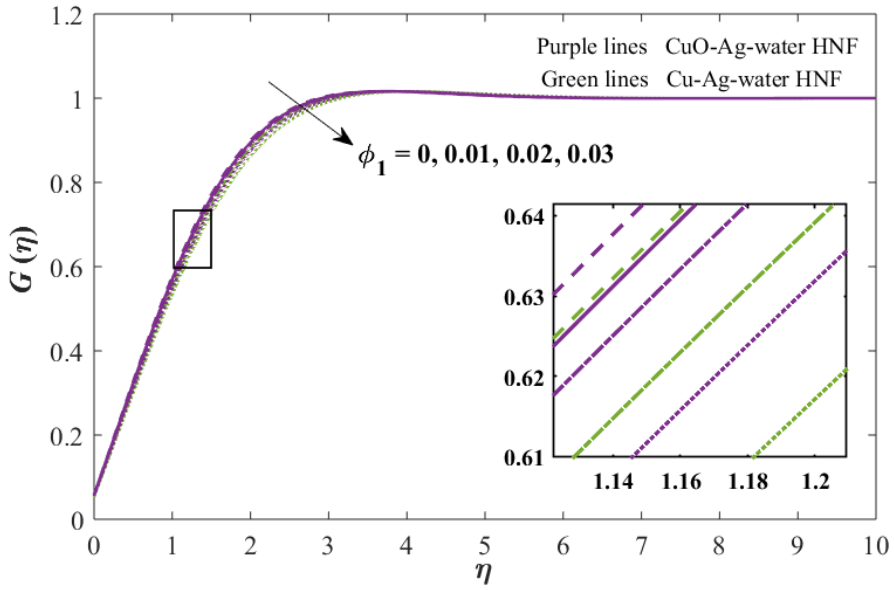

Figure 4.4: Behavior of $G(\eta)$ against ϕ_1

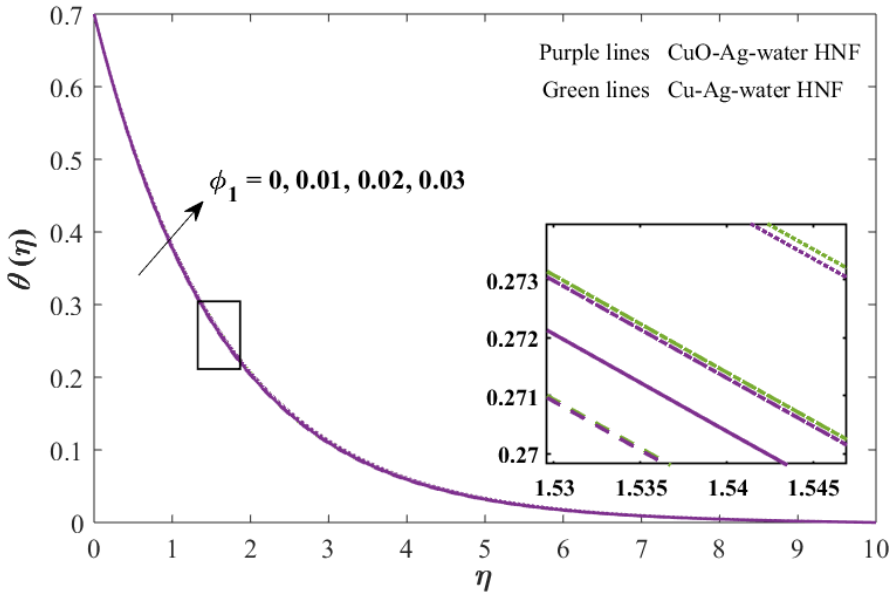

Figure 4.5: Behavior of $\theta(\eta)$ against ϕ_1

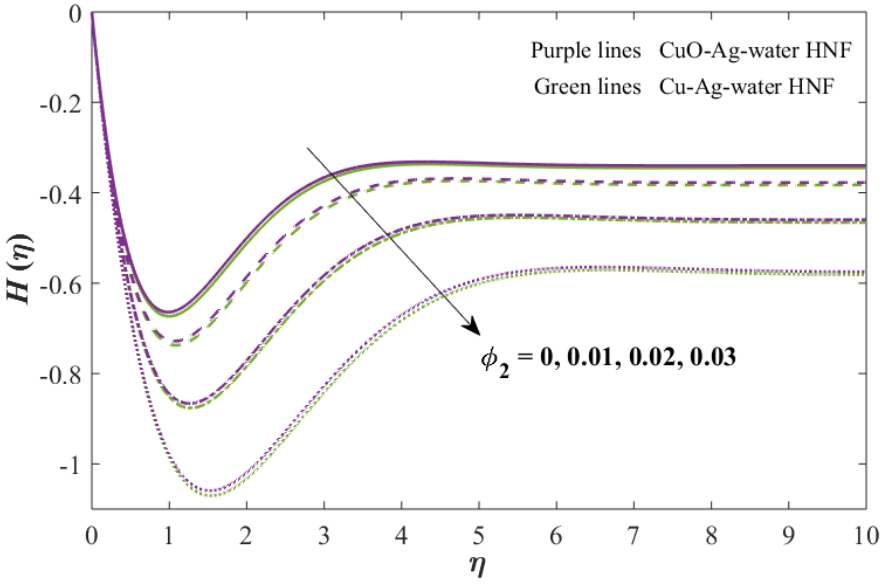

Figure 4.6: Behavior of $H(\eta)$ against ϕ_2

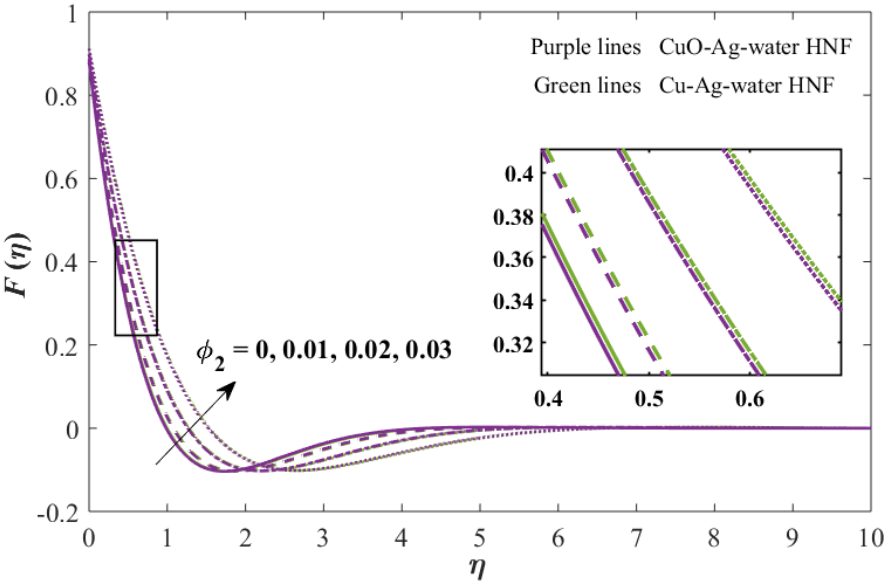

Figure 4.7: Behavior of $F(\eta)$ against ϕ_2

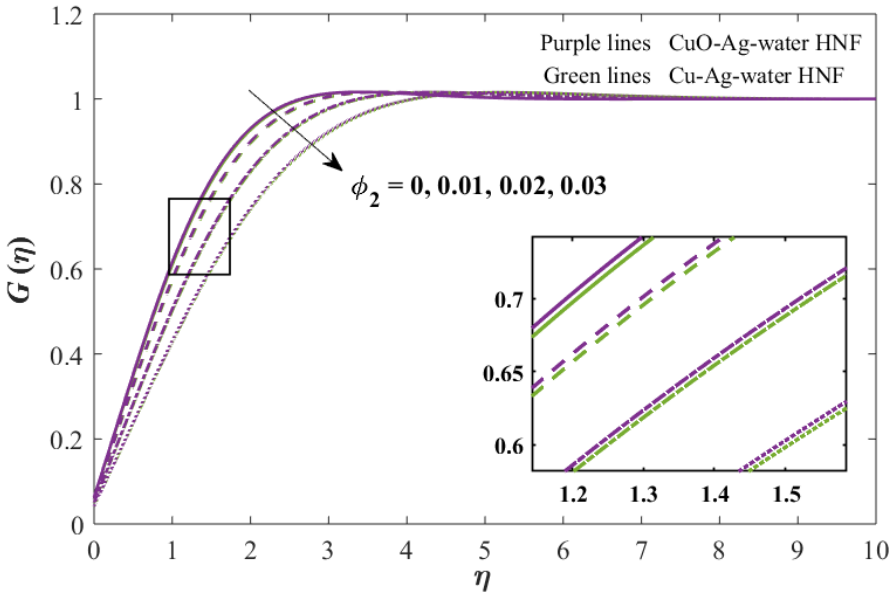

Figure 4.8: Behavior of $G(\eta)$ against ϕ_2

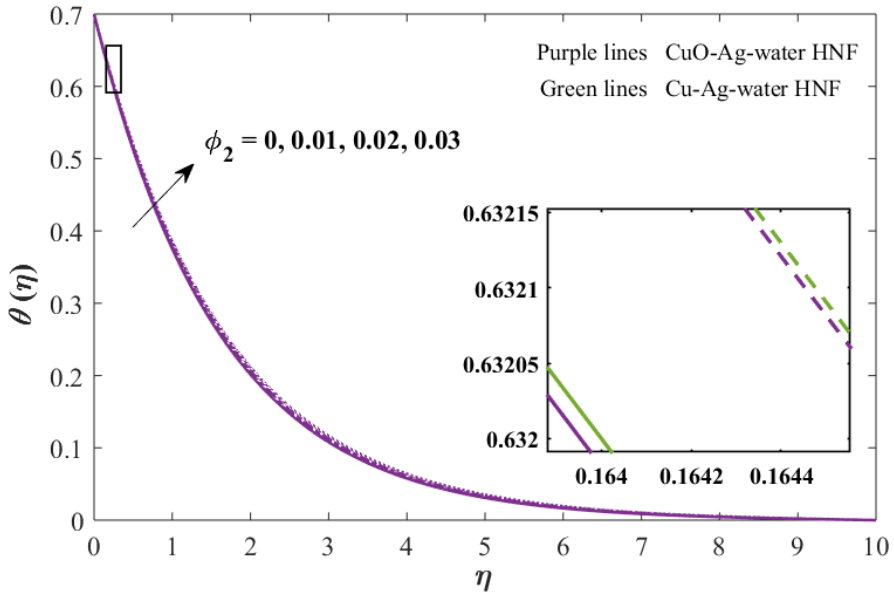

Figure 4.9: Behavior of $\theta(\eta)$ against ϕ_2

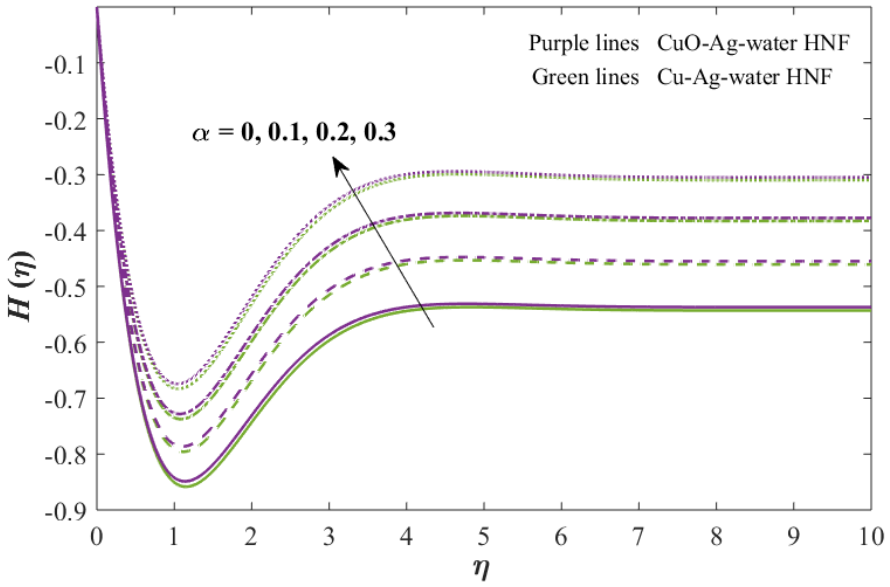

Figure 4.10: Behavior of $H(\eta)$ against α

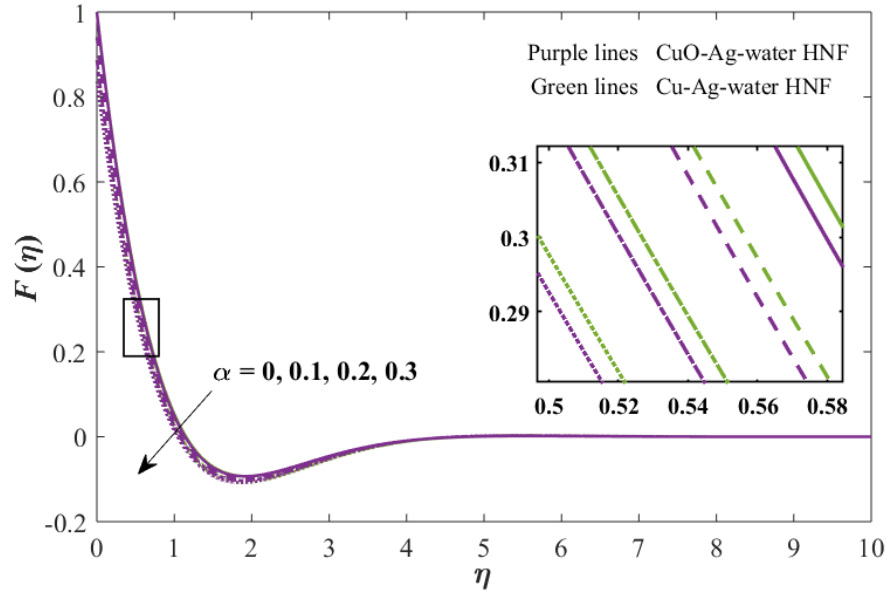

Figure 4.11: Behavior of $F(\eta)$ against α

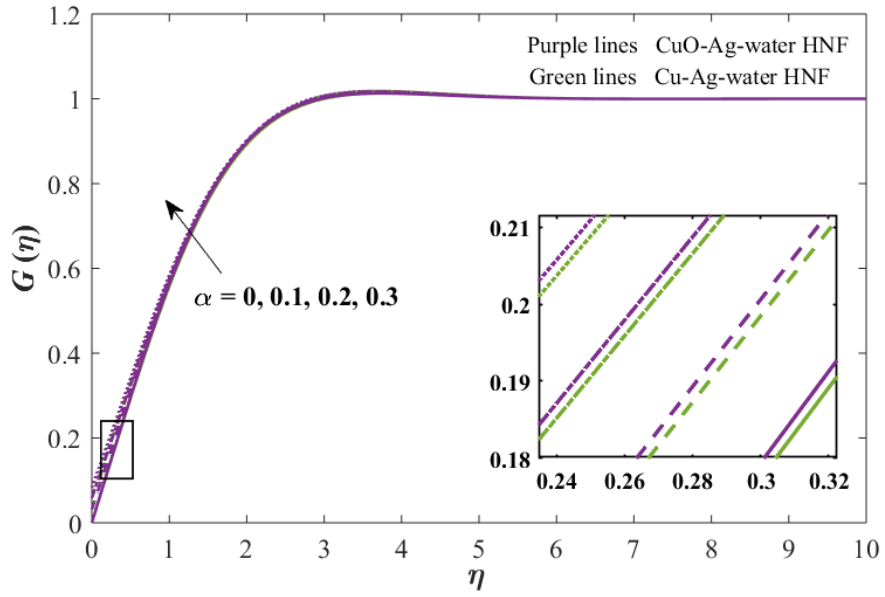

Figure 4.12: Behavior of $G(\eta)$ against α

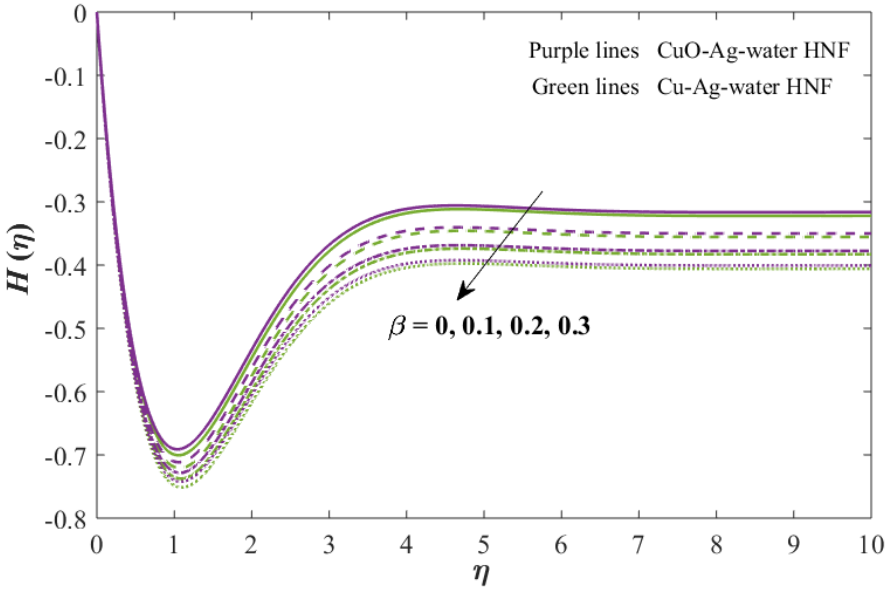

Figure 4.13: Behavior of $H(\eta)$ against β

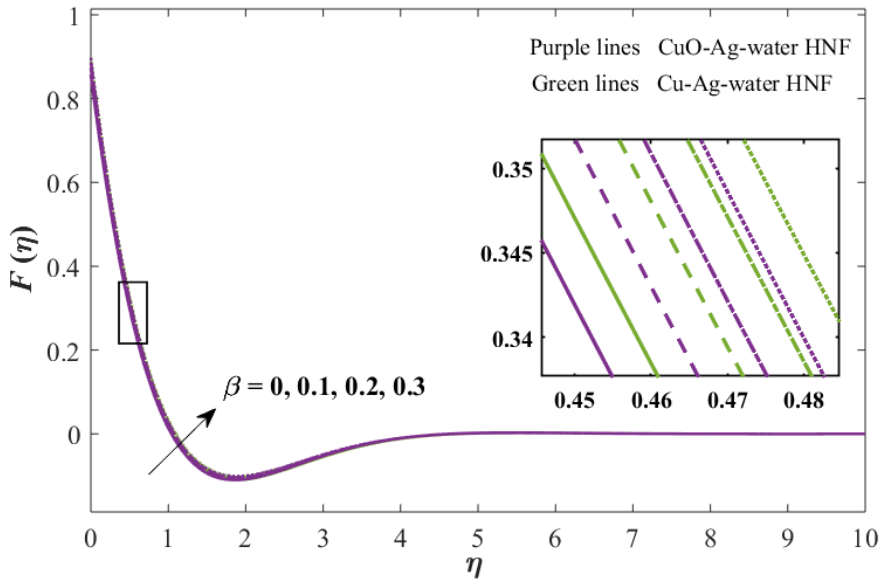

Figure 4.14: Behavior of $F(\eta)$ against β

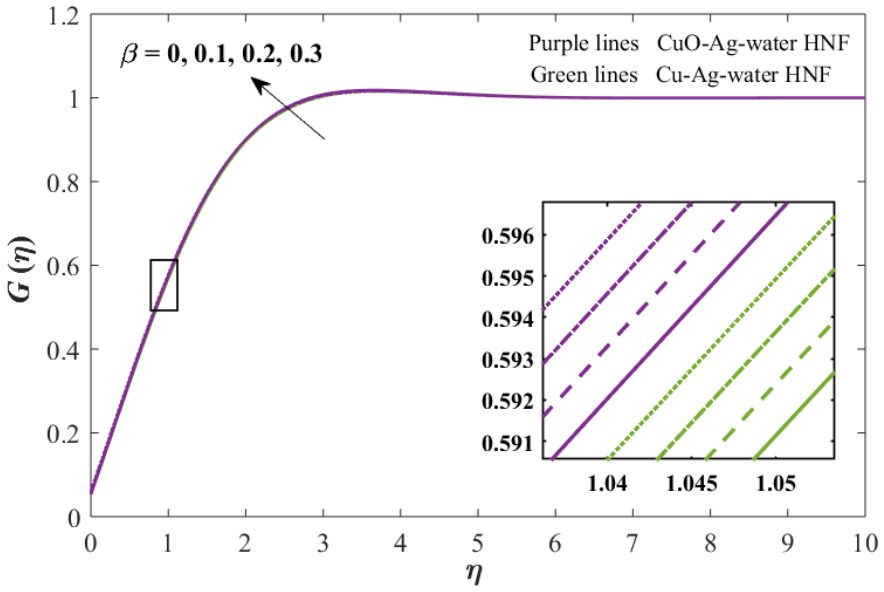

Figure 4.15: Behavior of $G(\eta)$ against β

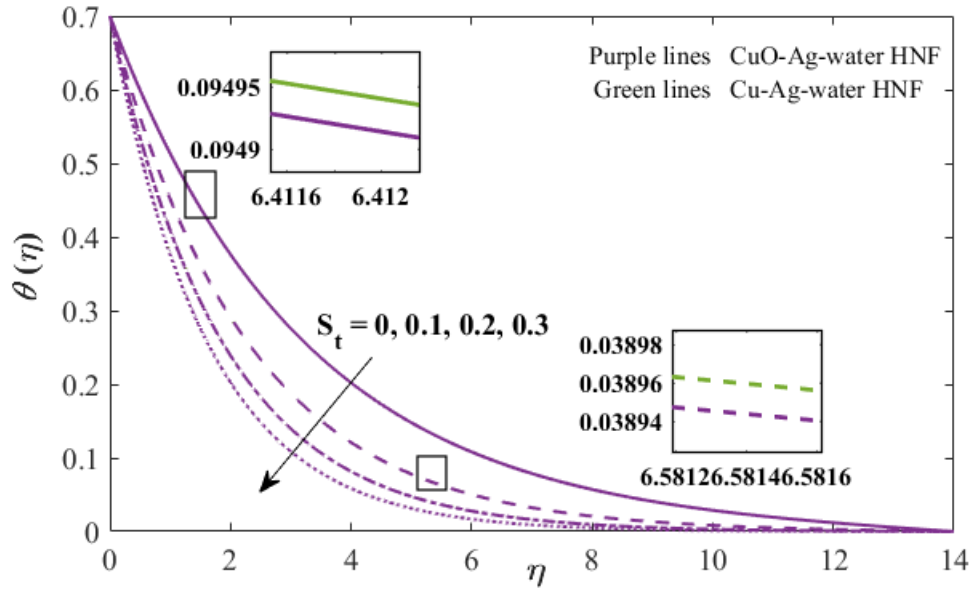

Figure 4.16: Behavior of $\theta(\eta)$ against S_t

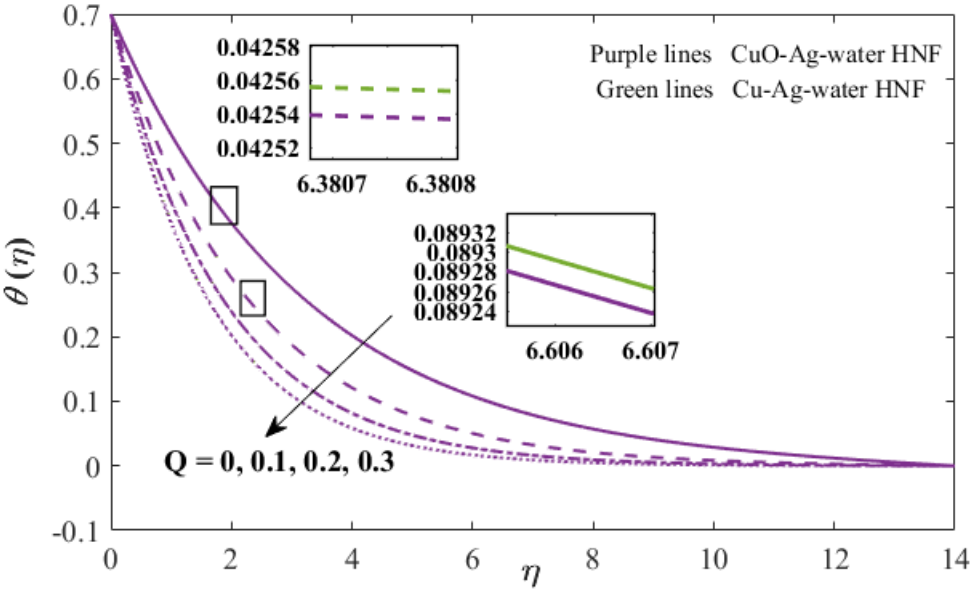

Figure 4.17: Behavior of $\theta(\eta)$ against Q

4.5 Skin friction and Nusselt number

The consequences of concentration of nanoparticles (ϕ_1, ϕ_2), heat source coefficient, thermal stratification variable and slip variables on $H(\infty)$, skin-friction in r-direction $(F'(0))$ and ϑ-direction $(G'(0))$ and Nu over a linear stretched disk in radial position are presented through tabular form in Table 4.2. Two different types of HNFs ($Cu-Ag-water$ and $CuO-Ag-water$) are taken into account in this research work, for first type of HNF two different shapes of NPs are taken i.e., Cu in spherical shape and Ag with cylindrical configuration and for second type of HNF CuO is in spherical structure and Ag along with cylindrical formation. Table 4.2 validates the consequence of nanoparticles volume fraction (ϕ_1, ϕ_2), heat source coefficient, thermal stratification variable and slip variables on $H(\infty)$ skin-friction in r-direction $(F'(0))$ and ϑ-direction $(G'(0))$ and rate of heat (Nu) for first type of HNF which is $Cu-Ag-water$. In this evaluation when we maximize ϕ_1 the values of variables of skin friction $F'(0)$ and $G'(0)$ minimizes and Nu maximizes while the opposite phenomenon is observed for the case of ϕ_2 when we increase its values. When we enhance the heat source Q, Nu increases which increases the heat transmission rate in the given system. When we enhance the S_t variable, Nu declines and heat transmission rate decreases. With the enhancement in α both skin-friction variables decrease in amount while with increasing the values of β, $F'(0)$ increases and $G'(0)$ decreases.

Table 4.2: Consequences of nanoparticles volume fraction (ϕ_1, ϕ_2), heat source coefficient, thermal stratification variable and slip variables on skin-friction in r-direction $(F'(0))$ and ϑ-direction $(G'(0))$ and rate of heat transport (Nu) for $Cu-Ag-water$ HNF

$Cu-Ag-water$ HNF									
ϕ_1	ϕ_2	Q	S_t	α	β	$H(\infty)$	$F'(0)$	$G'(0)$	Nu
0.01	0.01	0.4	0.3	0.2	0.2	-0.4342651	1.6545050	0.5937436	0.4513532
0.02						-0.4306628	1.6114339	0.5791413	0.4551263
0.03						-0.4257384	1.5913616	0.5729222	0.4603905
	0.01					-0.4342651	1.6545050	0.5937436	0.4513532
	0.02					-0.4269192	1.8104622	0.6535089	0.4591196
	0.03					-0.4185282	2.0471849	0.7427357	0.4683261
		0.1				-0.2172065	1.6545051	0.5937437	0.3149857
		0.2				-0.3070735	1.6545051	0.5937437	0.4526703
		0.3				-0.3760824	1.6545051	0.5937437	0.5568693
		0.4				-0.4342616	1.6545051	0.5937437	0.6440075
			0.1			-0.5583408	1.6545050	0.5937436	0.6445523
			0.2			-0.4963030	1.6545050	0.5937436	0.6442685
			0.3			-0.4342651	1.6545050	0.5937436	0.6440075
				0.1		-0.4342654	1.7407838	0.6300797	0.4513532
				0.2		-0.4342651	1.6545050	0.5937436	0.4513532
				0.3		-0.4342648	1.5766014	0.5636006	0.4513529
					0.1	-0.4342650	1.6370898	0.5969393	0.4513531
					0.2	-0.4342651	1.6545050	0.5937436	0.4513532
					0.3	-0.4342652	1.6687215	0.5901294	0.4513533

Table 4.3: Consequences of nanoparticles volume fraction (ϕ_1, ϕ_2), heat source coefficient, thermal stratification variable and slip variables on skin-friction in r-direction $(F'(0))$ and ϑ-direction $(G'(0))$ and rate of heat transport (Nu) for $CuO-Ag-water$ HNF

$CuO-Ag-water$ HNF									
ϕ_1	ϕ_2	Q	S_t	α	β	$H(\infty)$	$F'(0)$	$G'(0)$	Nu
0.01	0.01	0.4	0.3	0.2	0.2	-0.4343261	1.6716392	0.5996044	0.4512899
0.02						-0.4308247	1.6432183	0.5900544	0.4549553
0.03						-0.4260077	1.6363319	0.5884348	0.4600993
	0.01					-0.4343261	1.6716392	0.5996044	0.4512899
	0.02					-0.4269578	1.8277501	0.6595254	0.4590781
	0.03					-0.4185555	2.0653267	0.7491499	0.4682955
		0.1				-0.2172369	1.6716392	0.5996045	0.3149442
		0.2				-0.3071167	1.6716392	0.5996045	0.4526087
		0.3				-0.3761352	1.6716392	0.5996045	0.5567923
		0.4				-0.4343226	1.6716392	0.5996045	0.6439178
			0.1			-0.5584193	1.6716392	0.5996044	0.6444391
			0.2			-0.4963727	1.6716392	0.5996044	0.6441785
			0.3			-0.4343261	1.6716392	0.5996044	0.6439178
				0.1		-0.4343264	1.7595668	0.6366772	0.4512902
				0.2		-0.4343261	1.6716392	0.5996044	0.4512899
				0.3		-0.4343258	1.5923000	0.5689050	0.4512895
					0.1	-0.4343260	1.6537547	0.6029097	0.4512898
					0.2	-0.4343261	1.6716392	0.5996044	0.4512899
					0.3	-0.4343262	1.6862171	0.5958660	0.4512900

Table 4.3 validates the consequence of nanoparticles volume fraction (ϕ_1, ϕ_2), heat source coefficient, thermal stratification variable and slip variables on $H(\infty)$ skin-friction in r-direction $(F'(0))$ and ϑ-direction $(G'(0))$ and rate of heat (Nu) for second type of hybrid model which is $CuO-Ag-water$ HNF model. In this evaluation when we maximize ϕ_1 the behavior of skin friction $F'(0)$ and $G'(0)$ minimizes and Nu maximizes while the opposite phenomenon is observed for the case of ϕ_2 when we increase its values. When we enhance the heat source Q, Nu increases which increases the heat transmission rate in the given system. When we enhance the S_t variable, Nu declines and heat transmission rate decreases. With the enhancement in α both skin-friction variables decrease in amount while with increasing the values of β, $F'(0)$ maximizes and $G'(0)$ minimizes.

CHAPTER 5

CONCLUSION AND FUTURE WORK

5.1 Overview

This thesis examines two problems, the first of which is the review work of Mustafa [33] and the second of which is the extension work for it. The following are the main results for both problems.

The first problem was the review of Mustafa *et al.* [32] in which they studied the heat rate transmission of NFs past an immovable disk which is uniformly stretched in the radial direction by considering three different types of NPs of same formation i.e., CuO with spherical configuration, Cu in spherical shape and Ag with also spherical shape and BF H_2O. This research analysis represents the numerical approach on Bödewadt flow and heat transmission process in NFs. The famous Tiwari and Das model [21] is utilized in this research analysis for the given problem formulation. The current research yields the following results

- The nanoparticle volume fraction (ϕ) is a declining function of radial profile $F(\eta)$ and axial profile $H(\eta)$.
- When we increase the stretching of the uniformly stretched stationary disk in the radial direction, the BL thickness decreases in amount.
- When the rate of stretching in radial direction (s) of the stationary disk is significantly higher than the fluid rotation rate (Ω), the temperature parameter (θ) is reduced while NP volume fraction (ϕ) has a direct correlation with the temperature parameter (θ).

- The combination of copper oxide nanoparticle with BF water $(CuO-water)$ NF has a faster rate of heat transmission than the combination of copper nanoparticle with BF water $(Cu-water)$ NF and the combination of silver nanoparticle with BF water $(Ag-water)$ NF.
- As nanoparticle volume fraction (ϕ) increases, the upward component of velocity away from the boundary reduces in amount.
- The oscillatory properties of the radial velocity $F(\eta)$, axial velocity $H(\eta)$, and tangential velocity $G(\eta)$ distributions are reduced as the stretching in the radial direction on the stationary disk increases.

The second problem was extension of Mustafa *et al.* [32] which is in-depth research of thermally stratified Bödewadt flow of hybrid nanofluid (HNF) containing different shaped hybrid NPs past a stretching stationary disk surface including generalized slip condition having the effects of thermal stratification and heat source impacts is investigated. Two different hybrid models are considered in this research study which are $CuO-Ag-water$ HNF and $Cu-Ag-water$ HNF. Two different shaped NPs, which are CuO and Cu in spherical shape and Ag with cylindrical configuration are utilized in this research work. Uniqueness of this research work is supplemented by using the consequences of thermal stratification and heat source in thermally stratified Bödewadt flow of hybrid nanofluids. This study yields the following results

- The BL thickness reduces in quantity when the radial stretching rate is increased.
- An increase in the amount of NPs concentration (ϕ_1, ϕ_2), improves the HNFs temperature and due to this process the TBL augments as well.
- When we maximize the rotation parameter (Ω) and stretching parameter (C) the heat flow at the stationary disk surface also increases in amount.
- S_t reduces the system heat transfer rate.

- When we increase the amount of NP concentration (ϕ_1, ϕ_2), the axial velocity $H(\eta)$ and tangential velocity $G(\eta)$ decrease and the inverse impact can be seen for the consequence of radial velocity $F(\eta)$.
- With the enhancement in the variables of α, the axial profile $H(\eta)$ and the tangential velocity $G(\eta)$ of $CuO-Ag-water$ HNF flow enhances and declines for $Cu-Ag-water$ HNF flow.
- The temperature curve is a decreasing function of thermal stratification and heat source parameter.

5.2 Future work

For further work following may be considered

- The following BCs can be replaced by melting heat transmission and convective BCs.
- Linear and non-linear thermal radiation influences can also be considered.
- Cattaneo-Christov heat flux phenomena may also be considered.

REFERENCES

[1] Bödewadt, V.U., 1940. Die drehströmung über festem grunde. *ZAMM-Journal of Applied Mathematics and Mechanics/Zeitschrift für Angewandte Mathematik und Mechanik*, *20*(5), pp.241-253.

[2] Rafiq, T., Mustafa, M. and Farooq, M.A., 2019. Numerical assessment of Bödewadt flow and heat transfer over a permeable disk with variable fluid properties. *Physica A: Statistical Mechanics and its Applications*, *534*, p.122138.

[3] Muhammad, K., Hayat, T., Alsaedi, A. and Ahmad, B., 2020. Numerical study of entropy production minimization in Bödewadt flow with carbon nanotubes. *Physica A: Statistical Mechanics and its Applications*, *550*, p.123966.

[4] Awais, M., Bibi, M., Raja, M.A.Z., Awan, S.E. and Malik, M.Y., 2021. Intelligent numerical computing paradigm for heat transfer effects in a Bodewadt flow. *Surfaces and Interfaces*, *26*, p.101321.

[5] Mustafa, M., Rafiq, T. and Hina, S., 2021. Bödewadt flow of Bingham fluid over a permeable disk with variable fluid properties: A numerical study. *International Communications in Heat and Mass Transfer*, *127*, p.105540.

[6] Choi, S.U. and Eastman, J.A., 1995. *Enhancing thermal conductivity of fluids with nanoparticles* (No. ANL/MSD/CP-84938; CONF-951135-29). Argonne National Lab.(ANL), Argonne, IL (United States).7

[7] Joshi, V. K., Ram, P., Sharma, R. K., & Tripathi, D. (2017). Porosity effect on the boundary layer Bodewadt flow of a magnetic nanofluid in the presence of geothermal viscosity. *The European Physical Journal Plus*, *132*(6), 1-10.

[8] Khan, J. A., Mustafa, M., Hayat, T., & Alzahrani, F. (2017). Numerical study for Bödewadt flow of water based nanofluid over a deformable disk: Buongiorno model. *Indian Journal of Physics*, *91*(5), 527-533.

[9] Rafiq, T., Mustafa, M., & Khan, J. A. (2019). Numerical study of Bödewadt slip flow on a convectively heated porous disk in a nanofluid. *Physica Scripta*, *94*(9), 095701.

[10] Zhou, S. S., Ramzan, M., Howari, F., Kadry, S., Chu, Y. M., & Malik, M. Y. (2021). 3D Bio-convective nanofluid Bödewadt slip flow comprising gyrotactic microorganisms over a stretched stationary disk with modified Fourier law. *Physica Scripta*, *96*(7), 075702.

[11] Hayat, T., Muhammad, K., & Momani, S. (2021). Numerical study of entropy generation in Darcy-Forchheimer (DF) Bödewadt flow of CNTs. *International Journal of Hydrogen Energy*, *46*(69), 34449-34462.

[12] Hani, U., Khan, J. A., Rauf, A., Mustafa, F., & Shehzad, S. A. (2022). Bayesian and Numerical Techniques for Non-Newtonian Bödewadt Nanofluid Flow Above a Stretchable Stationary Disk. *Arabian Journal for Science and Engineering*, 1-15.

[13] Shah, Z., Rooman, M., Jan, M. A., Vrinceanu, N., Deebani, W., Shutaywi, M., & Bou, S. F. (2022). Radiative Darcy-Forchheimer Micropler Bödewadt flow of CNTs with viscous dissipation effect. *Journal of Petroleum Science and Engineering*, *217*, 110857.

[14] Hayat, T. and Nadeem, S., 2017. Heat transfer enhancement with Ag–CuO/water hybrid nanofluid. *Results in physics*, *7*, pp.2317-2324.

[15] Qiu, L., Zhu, N., Feng, Y., Michaelides, E.E., Żyła, G., Jing, D., Zhang, X., Norris, P.M., Markides, C.N. and Mahian, O., 2020. A review of recent advances in thermophysical properties at the nanoscale: From solid state to colloids. *Physics Reports*, *843*, pp.1-81.

[16] Abbas, N., Malik, M.Y., Alqarni, M.S. and Nadeem, S., 2020. Study of three dimensional stagnation point flow of hybrid nanofluid over an isotropic slip surface. *Physica A: Statistical Mechanics and its Applications*, *554*, p.124020.

[17] Muneeshwaran, M., Srinivasan, G., Muthukumar, P. and Wang, C.C., 2021. Role of hybrid-nanofluid in heat transfer enhancement–A review. *International Communications in Heat and Mass Transfer*, *125*, p.105341.

[18] Sahoo, B. (2011). Effects of slip on steady Bödewadt flow and heat transfer of an electrically conducting non-Newtonian fluid. *Communications in Nonlinear Science and Numerical Simulation*, *16*(11), 4284-4295.

[19] Sahoo, B., & Poncet, S. (2012). Effects of slip on steady Bödewadt flow of a non-Newtonian fluid. *Communications in Nonlinear Science and Numerical Simulation*, *17*(11), 4181-4191.

[20] Sahoo, B., Abbasbandy, S., & Poncet, S. (2014). A brief note on the computation of the Bödewadt flow with Navier slip boundary conditions. *Computers & Fluids*, *90*, 133-137.

[21] Abbas, Z., Rafiq, M. Y., Hasnain, J., & Nadeem, A. (2021). Thermally developed generalized Bödewadt flow containing nanoparticles over a rotating surface with slip condition. *International Communications in Heat and Mass Transfer*, *122*, 105143.

[22] Hayat, T., Qayyum, S., Alsaedi, A., & Shafiq, A. (2016). Inclined magnetic field and heat source/sink aspects in flow of nanofluid with nonlinear thermal radiation. *International Journal of Heat and Mass Transfer*, *103*, 99-107.

[23] Hayat, T., Khan, M., Khan, M. I., & Alsaedi, A. (2018). Entropy optimization and Sisko material flow with nonlinear radiative heat flux and heat source/sink. *Journal of the Brazilian Society of Mechanical Sciences and Engineering*, *40*(8), 1-12.

[24] Abdal, S., Siddique, I., Alshomrani, A. S., Jarad, F., Din, I. S. U., & Afzal, S. (2021). Significance of chemical reaction with activation energy for Riga wedge flow of tangent hyperbolic nanofluid in existence of heat source. *Case Studies in Thermal Engineering*, *28*, 101542.

[25] Irfan, M., Rafiq, K., Khan, M., Waqas, M., & Anwar, M. S. (2021). Theoretical analysis of new mass flux theory and Arrhenius activation energy in Carreau nanofluid with magnetic influence. *International Communications in Heat and Mass Transfer*, *120*, 105051.

[26] Awais, M., Bibi, M., & Ali, A. (2022). Numerical Treatment For MHD Axisymmetric Rotating Bodewadt Rheology Under Ohmic Heating And Viscous Dissipation Effects.

[27] Jafar, M. A., Abbas, Z., & Hasnain, J. (2021). Thermally stratified radiative flow of non-Newtonian fluid between two discs executing diverse type of in-plane motion. *Case Studies in Thermal Engineering*, *26*, 101187.

[28] Raza, M. A., Kanwal, Z., Rauf, A., Sabri, A. N., Riaz, S., & Naseem, S. (2016). Size-and shape-dependent antibacterial studies of silver nanoparticles synthesized by wet chemical routes. *Nanomaterials*, *6*(4), 74.

[29] Sobamowo, M. G., Akinshilo, A. T., & Yinusa, A. A. (2018). Thermo-magneto-solutal squeezing flow of nanofluid between two parallel disks embedded in a porous medium: effects of nanoparticle geometry, slip and temperature jump conditions. *Modelling and Simulation in Engineering*, *2018*.

[30] Dadsetani, R., Sheikhzadeh, G. A., Safaei, M. R., Leon, A. S., & Goodarzi, M. (2020). Cooling enhancement and stress reduction optimization of disk-shaped electronic components using nanofluids. *symmetry*, *12*(6), 931.

[31] Umavathi, J. C., Patil, S. L., Mahanthesh, B., & Bég, O. A. (2021). Unsteady squeezing flow of a magnetized nano-lubricant between parallel disks with Robin boundary conditions. *Proceedings of the Institution of Mechanical Engineers, Part N: Journal of Nanomaterials, Nanoengineering and Nanosystems*, *235*(3-4), 67-81.

[32] Mustafa, M., Khan, J. A., Hayat, T., & Alsaedi, A. (2015). On Bödewadt flow and heat transfer of nanofluids over a stretching stationary disk. *Journal of Molecular Liquids*, *211*, 119-125.

[33] Turkyilmazoglu, M. (2015). Bödewadt flow and heat transfer over a stretching stationary disk. *International Journal of Mechanical Sciences*, *90*, 246-250.

[34] Von Kármán, T. (1921). About laminar and turbulent friction. *Zeitschrift Angewandte. Mathematics and Mechanics. 1*, 233-252.

[35] Hasnain, J., & Abid, N. (2022). Numerical investigation for thermal growth in water and engine oil-based ternary nanofluid using three different shaped nanoparticles over a linear and nonlinear stretching sheet. *Numerical Heat Transfer, Part A: Applications, 1-12.*

[36] Tiwari, R. K., & Das, M. K. (2007). Heat transfer augmentation in a two-sided lid-driven differentially heated square cavity utilizing nanofluids. *International Journal of heat and Mass transfer*, *50*(9-10), 2002-2018.